Energy and Environment Division

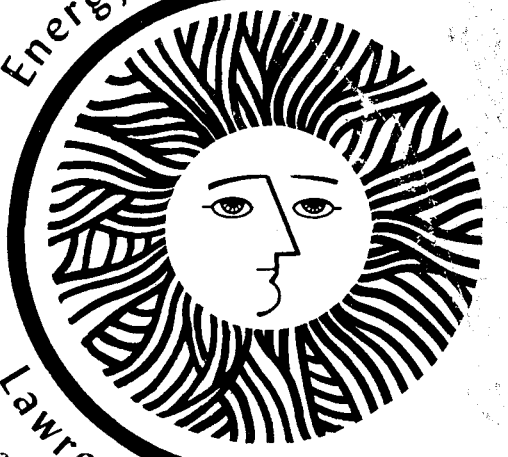

INVESTIGATION OF THE USE OF THE RESONANCE RAMAN EFFECT AS AN ENVIRONMENTAL MONITOR

Owen Chamberlain, Peter Robrish, and Hal Rosen

October 1976

Lawrence Berkeley Laboratory University of California/Berkeley

Prepared for the U.S. Energy Research and Development Administration under Contract No. W-7405-ENG-48

Final Report
NSF/RANN AG413
National Science Foundation
Washington, D.C.

LBL-5288

INVESTIGATION OF THE USE OF THE RESONANCE RAMAN EFFECT AS AN ENVIRONMENTAL MONITOR

Owen Chamberlain
Peter Robrish
Hal Rosen

Lawrence Berkeley Laboratory
University of California
Berkeley, California 94720

October 1976

This work was done with support from the U.S. Energy Research and Development Administration.

TABLE OF CONTENTS

Introduction

An essential element in any strategy designed to cope effectively with atmospheric pollution is the development of more sensitive or more convenient methods for determining the concentrations of pollutant gases in ambient air and in emissions from localized sources. One general class of methods for measuring pollutant concentrations makes use of lasers to probe the atmosphere remotely and obtain spectroscopic information about the molecules present in the segment of atmosphere under consideration. In particular, the use of a laser to measure the Raman spectra of molecular constituents remotely seems to offer some promise of being an effective monitor of gaseous pollutants. This scheme, called Raman Lidar, is implemented in a manner analogous to the use of a radar system. A laser transmitter directs a pulsed beam into the atmosphere. By measuring the time between the initial laser pulse and the returning signal, one determines the range of the atmospheric region being monitored. The light coming from this region is spectroscopically analyzed. The Raman spectrum, which is due to transitions between vibrational states of a molecule, is a unique signature for a particular molecular species. Therefore, a measurement of its intensity allows one to determine the concentration of that molecule in the region of interest.

Raman Lidar allows one, in principle, to make a three-dimensional map of molecular concentrations in real time with good spatial resolution out to a distance of several kilometers from a fixed transmitter. In fact, Raman Lidar systems have been used for some time to study major atmospheric constituents.[1] However, the fact that Raman cross sections are quite small ($\sim 10^{-30}$ cm^2/sr) has made this technique difficult to use to detect minor

atmospheric constituents such as pollutants. In spite of this difficulty, S. Nakahara et al.[2] and Melfi et al.[3] have reported detection of SO_2 in power plant stack plumes at a range of 200 m at night, and Hirschfeld et al.[4] using a powerful doubled ruby laser have been able to measure SO_2 concentrations of 30 ppm at 200 m in full daylight with a good signal-to-noise ratio.

It is well known that Raman cross sections are enhanced if the laser source is tuned close to an absorption line in a gas. Since such enhancements could dramatically increase the sensitivity of a Raman Lidar system, we have been investigating the resonance Raman effect[5] to determine its usefulness in such a system. This final report on our study of the feasibility of resonance Raman scattering as an environmental monitor will consist of three parts. The first section will detail the major conclusions of the study as they apply to remote detection of pollutant gases. The experimental work in molecular spectroscopy which underlies the conclusions presented in Section I will be presented in Section II, and in Section III we will describe various activities which were either necessary for our primary objective, or grew out of the development work which we carried out in pursuit of that objective.

SECTION I

FEASIBILITY OF THE REMOTE DETECTION OF POLLUTANTS USING RESONANCE RAMAN SCATTERING

As a major part of this project we have carried out an extensive search for large enhancements of scattering into the ν_2 Raman mode of NO_2 using a nitrogen-laser-pumped dye laser. The details of this investigation are presented in Section II. We have seen large resonance enhancements, and have measured a cross section of 5.6×10^{-27} cm^2/sr for narrow band ($\sim$1 Å) reemission into the ν_2 Raman mode at the peak of one of the resonances for 1 mm of NO_2 plus 1 atm of N_2 buffer gas. We have also measured a resonance Raman cross section of 1.7×10^{-24} $cm^2/ster$ for I_2 in 1 atm of N_2 (See Section II.). Penny et al.[6] have observed a large enhancement for the ν_1 Raman mode of SO_2 and measured a cross section of 10^{-25} $cm^2/ster$ for SO_2 in 700 mm of air. These cross sections are several orders of magnitude larger than the Raman cross section for N_2 at equivalent excitation wavelengths. Resonant inelastic scattering cross sections[7] of the order of 10^{-20} to 10^{-21} cm^2/sr have also been observed for OH,[8,9] and Wang and Davis[9] were able to measure atmospheric concentrations of OH at a level of 2 parts in 10^{13}. All of these measurements, along with the results of the following calculation, allow one to make reasonable estimates of the sensitivity of a resonance Raman Lidar system.

One can easily estimate the resonance Raman cross section for diatomic molecules which have known oscillator strengths and Franck-Condon factors. For a single frequency exciting laser operated near an isolated absorption line, the cross section can be written approximately as[10]:

$$\frac{d\sigma}{d\Omega} \cong \frac{\gamma_T}{\gamma_T - \gamma_e} \frac{e^4 \omega_\ell \omega_s^3 |\langle I|r|M\rangle|^2 |\langle M|r|F\rangle|^2 \rho_I}{\hbar^2 c^4 [(\omega_\ell - \omega_o)^2 + \gamma_T^2]} \qquad (1)$$

where $\langle I|r|M\rangle$ is the matrix element from the initial to intermediate vibrational-rotational state, while $\langle M|r|F\rangle$ is the matrix element between the intermediate and final state. ω_ℓ is the laser frequency, ω_s the scattered frequency, ω_o the central frequency of the resonance, and ρ_I is the relative thermal population of the initial vibrational-rotational state. γ_T is the pressure broadened line width while γ_e is the partial width due to elastic collisions. This expression is valid if γ_T is larger than the line width due to the combination of natural, doppler, and hyperfine broadening. For most molecules at atmospheric pressure the line width is, in fact, primarily due to pressure broadening.

We can rewrite Eq. (1) in terms of the oscillator strength, f, and the Franck-Condon factors, S_{ij}, by making the substitution

$$|\langle I|r|M\rangle|^2 = \frac{\hbar}{2m\omega_o}\,\frac{f\,S_{IM}}{3}$$

$$|\langle M|r|F\rangle|^2 = \frac{\hbar}{2m\omega_o}\,f\,S_{MF}$$

The factor of 3 in the first matrix element occurs because we assume that the oscillator strength is equally divided between the P, Q, and R branches of the absorption line. For $\omega_\ell = \omega_o \approx \omega_s$ [11] we get:

$$\frac{d\sigma}{d\Omega} \cong \frac{r_o^2\,\omega_s^2\,S_{IM}\,S_{MF}\,f^2\,\rho_I}{12\gamma_T^2} \qquad (2)$$

where r_o is the classical radius of the electron and we have assumed γ_T is dominated by inelastic collisions. While this last assumption may not

be valid, it leads to an expression which yields a lower limit for the cross section. For molecules where the oscillator strengths and Franck-Condon factors are known,[12-22] we can use Eq. (2) to make an estimate of the resonance Raman cross sections. We assume that the molecules are initially in their ground vibrational state and choose the intermediate and final vibrational states to maximize $S_{IM}S_{MF}$. We also choose the initial rotational state with the maximal thermal population and use standard methods to calculate ρ_I.[23] We choose γ_T on the basis of our work with I_2 where we found $\gamma_T = 2 \times 10^{10}$ radians/sec for 1 mm of I_2 in 1 atm of N_2 (See Section II.). The results of these calculations as well as experimentally determined cross sections are presented in Table I. It should be noted that our calculation of the resonance Raman cross section for I_2 is in very good agreement with the experimentally determined value. This gives us some confidence in our calculation of the cross sections for the other diatomic molecules shown in the table.

Using these cross sections we may deduce the effect of resonantly enhanced Raman cross sections for pollutant detection by means of a Lidar system. For such a system, the number of signal photons detected is:

$$S = 2.69 \times 10^5 \, \eta N \frac{E}{\hbar\omega_o} \frac{AL}{R^2} \rho \frac{d\sigma}{d\Omega} e^{-[\alpha_s+\alpha_o]R} \qquad (3)$$

with

η = total detection efficiency (optical and quantum efficiency)

N = number of laser pulses

E = laser pulse energy (joules)

ω_o = laser frequency (radians/sec)

Table I. Resonance Raman cross sections for various small molecules in 1 atm of nitrogen determined either experimentally or from Eq. (2).

Molecule	Electronic Transition	Vibrational Transition	λ_L(Å)	$\frac{d\sigma}{ds}$(cm^2/ster)$_{calc.}$	$\frac{d\sigma}{ds}$(cm^2/ster)$_{exp.}$	Refs.
CO^+	$A\ ^2\Pi_i - X\ ^2\Sigma^+$	0-1, 1-1	4913.0	2.5×10^{-20}		12
SO	$A\ ^3\Pi_0 - X\ ^3\Sigma^-$	0-2, 2-0	2579.0	1.3×10^{-20}		13
OH	$A\ ^2\Sigma^+ - X\ ^3\Pi_i$	0-0, 0-1	3064.0	2.4×10^{-22}	$10^{-20} - 10^{21}$ (7)	14,15
NO	$A\ ^2\Sigma^+ - X\ ^2\Pi$	0-0, 0-3	2262.0	1.3×10^{-23}		16,17
I_2	$B\ ^3\Pi^+_{Ou} - X\ ^1\Sigma^+_g$	0-25, 25-1	5466.36	1.2×10^{-24}	1.7×10^{-24}	18,19
SO_2	$\tilde{A}\ (^1B_1) - \tilde{X}\ ^1A_1$		2999.6		1×10^{-25}	6
$^{79}Br^{81}Br$	$B\ ^3\Pi^+_{Ou} - X\ ^1\Sigma^+_g$	0-28, 28-1	5264.0	7.8×10^{-27}		20,21
NO_2	$\tilde{A}\ (^2B_1) - \tilde{X}\ ^2A_1$(?)		4547.4		5.6×10^{-27}	
CO	$a\ ^3\Pi - X\ ^1\Sigma^+$	0-0, 0-1	2063.0	4.5×10^{-30}		12
Cl_2	$A\ ^3\Pi^+_{Ou} - X\ ^1\Sigma^+_g$	0-15, 15-3	4933.0	7×10^{-31}		20,22

LBL-5288

A = collector area (cm^2)

L = range increment (m)

R = range (km)

ρ = concentration of pollutant (ppm)

$\frac{d\sigma}{d\Omega}$ = Raman scattering cross section (cm^2/sr)

α_o = atmospheric absorption coefficient at laser frequency

α_s = atmospheric absorption coefficient at scattered frequency

The number of counts collected during the same number of pulses from skylight is:

$$B = \eta N \frac{W(\omega_s)\Delta\lambda}{\hbar\omega_s} A \phi \frac{2L}{c} \qquad (4)$$

with

$W(\omega_s)$ = background irradiance at the scattered wavelength (watts/cm^2 sr Å)

$\Delta\lambda$ = detector bandwidth (Å)

ϕ = detector field of view (sr)

ω_s = Raman shifted frequency

$\frac{2L}{c}$ = gate time for range increment (sec)

A useful measure of the sensitivity of a Lidar system can be obtained by considering the signal-to-noise ratio (SNR). When detecting scattered light with wavelength >3000 Å, we will assume that the noise is dominated by the fluctuations in the background irradiance, so that SNR = $S/\sqrt{B}$. For detection at wavelengths <3000 Å, where the stratospheric ozone layer effectively absorbs sunlight, and for nighttime detection, we will assume that the noise is caused by fluctuations in the signal, so that SNR = $\sqrt{S}$.

We ignore the possible problems associated with additional background due to the fluorescence of aerosols.[24] This background may cause trouble for a Lidar system which depends on ordinary Raman scattering. However, since the useful resonance cross sections are at least 3 orders of magnitude larger than ordinary Raman cross sections, we feel justified in ignoring this problem for the purposes of our illustrative calculations.

Our point of view in this calculation has been to make technological assumptions which are at the limits of present capability and to balance these assumptions by requiring the system to meet strict eye safety standards and to give a measurement of pollutant concentration accurate to 10% with a range resolution of 10 m. Our model Lidar system is, therefore, technically feasible, though perhaps not economically feasible at present. The most technologically sophisticated results that we have seen in the literature are those of Hirschfeld et al.[4] who built a detector with $A = 6.6 \times 10^3$ cm^2 and $\Delta\lambda \simeq 5$ Å. From their results on Raman scattering from N_2, one can estimate an overall detection efficiency of $\sim$3%. We assume $A = 10^4$ cm^2, $\eta = 0.1$, $\Delta\lambda = 1$ Å, and $\phi = 10^{-5}$ sr for our calculation. The choice of a 1-Å bandwidth is based on the fact that narrow band filters with good transmission are now available throughout most of the visible region and that for a Lidar system detecting radiation in the solar blind region below 3000 Å, a narrow band interference filter is not necessary. The large value of η may be optimistic for a field instrument; however, a glance at Eqs. (3) and (4) will show that SNR only depends on $\eta^{1/2}$. We assume a laser transmitter which emits a beam of 10^3 cm^2 cross-sectional area and limit the laser energy to .05 mJ/pulse for a repetition rate of

100 Hz in order to comply with the laser safety standard for direct viewing.[25] This limitation applies for lasers with wavelengths >4000 Å. For shorter wavelengths, the limits appear to be less stringent, but since there are no standards for very short pulses, we will assume the same standard as for wavelengths >4000 Å. We use the data of Baum and Dunkelman[26] to evaluate α_o, α_s, and that of Knestrick and Curcio[27] for $W(\omega_s)$. We further assume a range resolution of 10 m and calculate the concentration of pollutant which yields SNR = 10 with an integration time of 100 sec. In Figure 1, we present the results of that calculation for NO_2, SO_2, and NO using the cross sections in Table 1.

Figure 1 shows that, with the marginal exception of daylight detection of NO_2, a Lidar system making use of resonance Raman scattering can easily detect the pollutant concentrations typical of smoke plumes (>10 ppm) at a range of a few hundred meters using lasers with only very modest energies. A useful comparison can be made with the recent report[4] of detection of SO_2 using ordinary Raman scattering. In that case, the laser used had an average power of 0.4 W and an energy/pulse of 0.2 J, and was able to detect 30 ppm at 200 m with SNR $\sim$ 10. Our calculation shows that using a laser of 5 mW average power and 0.05 mJ/pulse, one could achieve a sensitivity of a factor of 10 better by making use of the resonance Raman effect. In addition, if there is an enhanced cross section in SO_2 for λ_o < 2800 Å, comparable to that for λ_o = 2999.6 Å, then the resonance Raman Lidar sensitivity for daylight detection of SO_2 will be the same as for nighttime detection, since sky background interference with the detected radiation will no longer be a problem. The fact that the SO_2 absorption spectrum

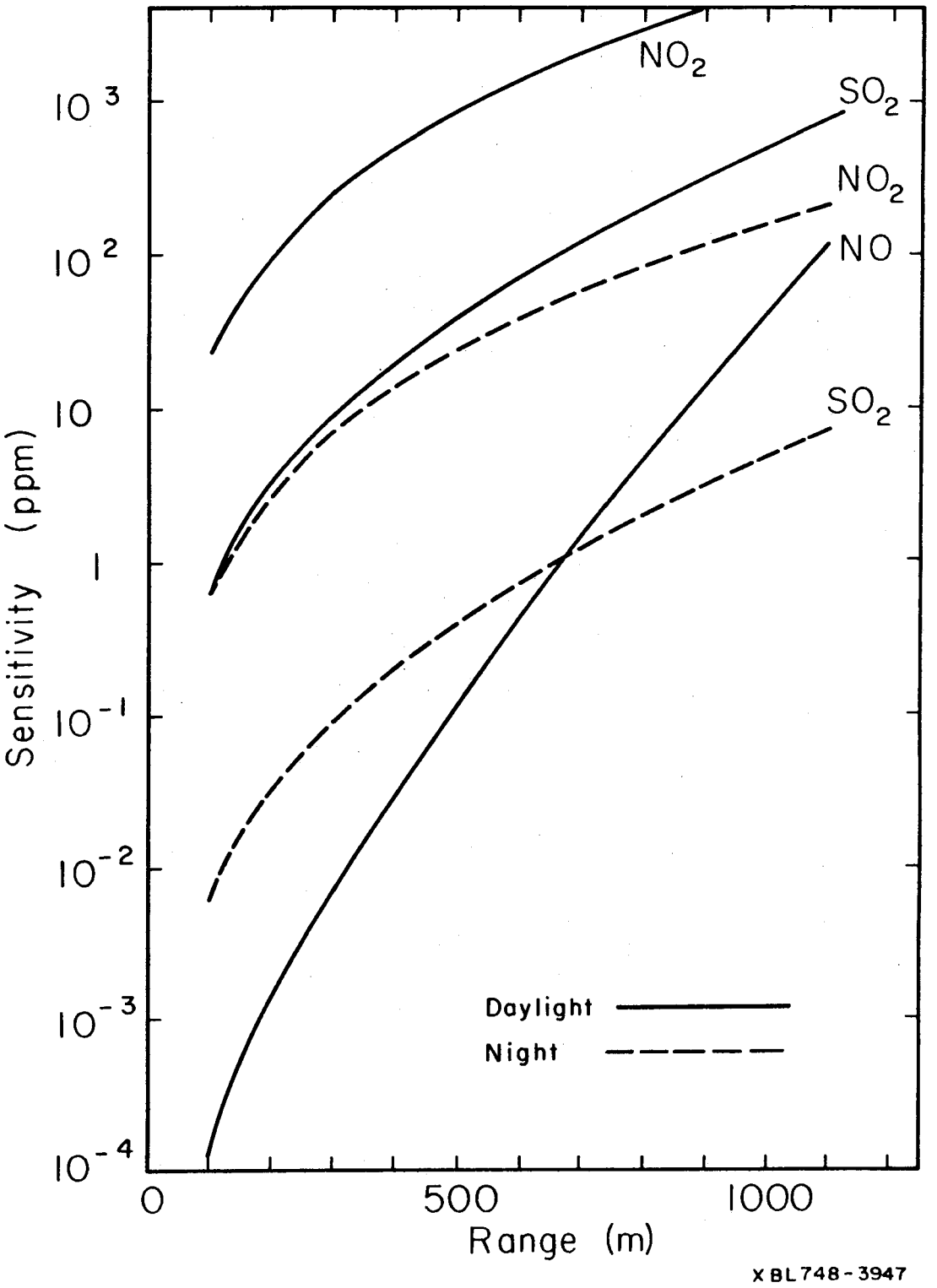

Figure 1. Lidar sensitivity vs range for E = 0.05 mJ and N = 10^4 pulses assuming a signal-to-noise ratio of 10 and a visibility of 10 km.

shows features at $\lambda < 2800$ Å similar to that at $\lambda \sim 3000$ Å leads one to expect that comparable enhancements will be found for such wavelengths.

Using presently available technology, one could construct a nitrogen-laser-pumped dye laser which has the required pulse energy and repetition rate[28] and by using nonlinear doubling crystals could extend its tuning capability to ∿2300 Å.[29] In order to detect NO, however, one needs a laser at 2260 Å. At present, the nonlinear crystals available for frequency doubling to this wavelength have conversion efficiencies of <1%.[30] However, at least one efficient technique for up-conversion of light with $\lambda > 2500$ Å to span the wavelength region 2000-2350 Å has been reported.[31] It should be noted that even if the efficiency of conversion of visible light to light at 2260 Å were only ∿0.01%, there would still be enough sensitivity to monitor NO in smokestacks at ∿200 m.

Figure 1 also shows that monitoring of ambient concentrations (∿0.1 ppm) at distances of the order of 1 km is certainly out of the question, given the safety constraint we have imposed on the calculation. If one could be sure that there would be no eye exposure to the light from the Lidar transmitter, then one might be able to use high-energy tunable lasers to gain the required sensitivity.

It seems to us that the advantages in sensitivity and safety associated with the use of resonance enhancements in a Raman Lidar system outweigh the additional problems associated with the use of a tunable laser as a Lidar transmitter. The fact that an instrument for use in populated areas will probably have to comply with stringent eye safety standards implies that the use of resonance enhancements may be the only avenue to a workable Raman Lidar system for remote smokestack monitoring.

SECTION II

MOLECULAR SPECTROSCOPY

Resonance Raman Scattering in I_2 Vapor

We chose to investigate resonance Raman scattering in I_2 vapor for our initial experiments. There have been several studies of resonance enhancements in iodine using the accidental coincidences between I_2 absorption lines and argon and krypton laser wavelengths. However, these studies[32] have given inconsistent results for the magnitude of the enhancements as well as for the quenching of the scattering with the addition of nitrogen.

We have investigated resonance Raman scattering in I_2 vapor for several of the strongest rotational absorption lines in the 0-25 vibrational band of the B-X electronic transition with a narrow-band pulsed dye laser. We decided to investigate this band because the product of the matrix elements for absorption and inelastic reemission is the largest of the B-X system. (The Franck-Condon factors were obtained from J. Tellinghuisen in a private communication.) Our effort has concentrated on the 0-25 P(47) rotational line which is relatively isolated from other absorption lines. For this line we have measured the resonance Raman cross section versus nitrogen buffer gas pressure for various laser frequencies.

The experimental arrangement consisted of the usual 90° scattering geometry, a Jarrell-Ash double monochromator, and a gated electrometer (See Section III.) which integrated the charge from an RCA 8575 photomultiplier tube. The exciting source was a nitrogen-laser-pumped dye laser similar to that of Hänsch[33] using a 5×10^{-3} molar solution of fluorescein disodium salt in ethanol. The bandwidth of the laser was narrowed by using a beam expanding telescope and a 1-cm^{-1} air spaced

etalon in series with a grating which constituted an end mirror of the laser cavity. The grating was blazed at 61° and operated in fifth order. In this configuration, the laser had a line width of 0.037 ± 0.007 cm^{-1} and an average power of 0.2 mW. A unique feature of our laser design was the scheme used for fine tuning. The etalon and the grating were enclosed in a vacuum tight chamber and the frequency was tuned by varying the pressure within the chamber. The advantage of pressure tuning is that the bandpass of the etalon remains centered on that of the grating without mechanical manipulation of either the grating or the etalon. Using pressure tuning we have been able to tune over an interval of 3 cm^{-1} in steps of 0.01 cm^{-1} in a stable and reproducible manner.

In Figure 2 we show a plot of the integrated intensity of the first Raman mode of I_2 versus laser frequency. The spectrum was taken by centering the spectrometer bandpass (75 cm^{-1}) on the Stokes Raman mode at $\sim$213 cm^{-1} and then pressure tuning the laser. The sample cell contained I_2 at its room temperature vapor pressure (0.28 mm) with no buffer gas present. The laser beam was attenuated and defocused sufficiently to avoid saturation and heating effects. The peaks in the scattered intensity correspond within experimental error to peaks in the absorption spectrum.[34] As one approaches an absorption line, the cross section increases dramatically. For example, at the peak of the 0-25 P(47) transition, the differential scattering cross section, $\frac{d\sigma}{d\Omega}$, was measured to be 8.3×10^{-21} cm^2/ster which is over 10 orders of magnitude larger than the Raman cross section for nitrogen at 5460 Å.[35] The cross sections were calculated by using the cross section for the 992 cm^{-1} mode of benzene[36] as a standard and making small corrections for absorption and spectral efficiency.

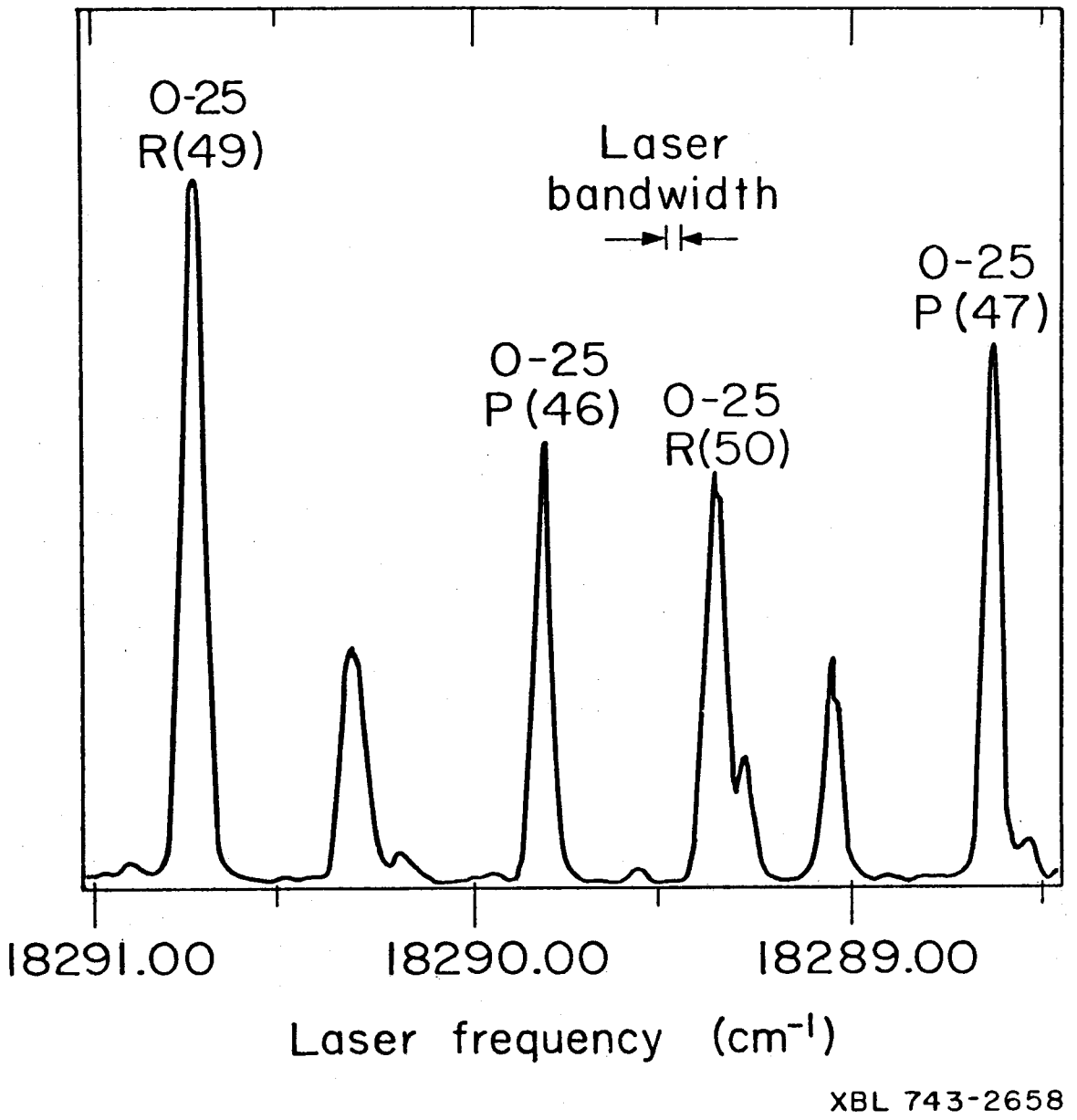

Figure 2. Scattered intensity of Raman mode located at ∿213 cm^{-1} vs laser frequency for I_2 vapor at a pressure of 0.28 mm with no buffer gas present.

We have investigated the quenching of the scattering cross section by nitrogen near the 0-25 P(47) transition. This transition, in contrast to the 0-43 P(12), R(14) transitions investigated by previous authors[32] has very little structure within 0.4 cm^{-1} of its high frequency side (See Fig. 2.). In Figure 3 we show a plot of the resonance Raman cross section versus nitrogen pressure for several different laser frequencies. For all measurements, both the incident laser beam and the scattered light accepted by the spectrometer were polarized perpendicular to its entrance slit. The bandpass of the spectrometer was set to 75 cm^{-1}. With the laser set on resonance, the cross section is quenched by over a factor of 1000 for a change in N_2 pressure from 2 mm to 730 mm. As one tunes off resonance, the quenching becomes progressively smaller until at 0.2 cm^{-1} away from the absorption line there is virtually no quenching.

We can gain some qualitative understanding of the results of this experiment by considering the effects of foreign gas collisions on the Rayleigh scattering from a two-level system treated in the impact approximation. One can show that the amount of scattered radiation is proportional to the population in the upper state and therefore to the energy stored in the two-level system. For a system which initially is in the ground state, the stored energy varies with time as $\sin^2 \frac{\Delta\omega}{2} t$ where $\Delta\omega$ is the angular frequency difference between the incident light and the resonance frequency of the two-level system. For a system which initially has some stored energy, there is an additional constant term. Now, for inelastic collisions, the system loses its stored energy with each collision, so that during the time between collisions, τ_c, it behaves as $\sin^2 \frac{\Delta\omega}{2} t$. Under these conditions, and for $\Delta\omega \gg 1/\tau_c$, there are many oscillations

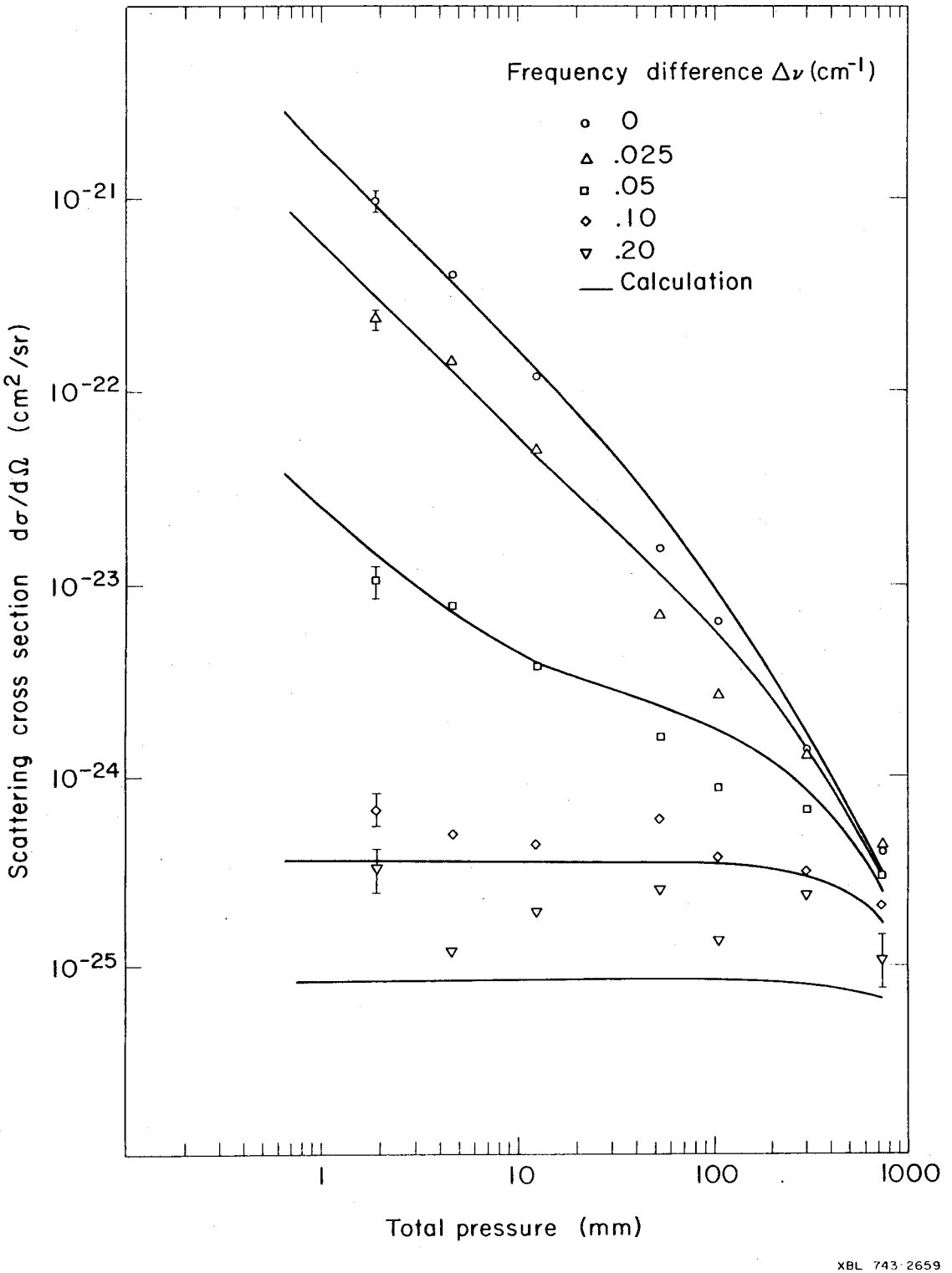

Figure 3. Plot of the differential resonance Raman scattering cross section for the Raman mode located at ∿213 cm^{-1} vs nitrogen buffer gas pressure for laser frequencies separated from the center of the 0-25 P(47) rotational line by 0, 0.025, 0.05, 0.1, and 0.2 cm^{-1}.

of the stored energy between collisions so that the effect of (inelastic) collisions on the average value of the stored energy $\bar{E}_s$ is small, while for $\Delta\omega \ll 1/\tau_c$ the effect on $\bar{E}_s$ will be large and the scattered radiation will be quenched significantly. This simple picture is complicated by the effects of elastic collisions which randomize the phase of the wave function with respect to the driving field, but do not change the instantaneous value of the energy. Elastic collision will have a significant effect on $\bar{E}_s$ for both $\Delta\omega \gg 1/\tau_c$ and $\Delta\omega \ll 1/\tau_c$. In fact, for $\Delta\omega \gg 1/\tau_c$, $\bar{E}_s$ increases with each elastic collision, while for $\Delta\omega \ll 1/\tau_c$ it decreases. If, however, we ask how the system behaves as a function of increased foreign gas pressure, then as long as the ratio of elastic to inelastic collision rates is not a function of pressure, there is still no quenching for $\Delta\omega \gg 1/\tau_c$ because the average number of elastic collisions occurring before an inelastic collision remains fixed and therefore $\bar{E}_s$ remains unchanged.

We can also make a quantitative comparison of our data to theory, but the analysis is complicated by the Doppler and hyperfine broadening of the absorption line and the line width of the laser. Near an isolated absorption line, the resonance Raman cross section in the impact approximation can be written as[10]:

$$\frac{d\sigma}{d\Omega} \propto \frac{\Gamma_T}{\Gamma_T - \Gamma_e} \int_0^\infty S(\nu_\ell - \nu_\ell{}^0)d\nu_\ell \int_0^\infty \frac{G(\nu_r - \nu_r{}^0)d\nu_r}{(\nu_\ell - \nu_r)^2 + \Gamma_T{}^2}$$

where $G(\nu_r - \nu_r{}^0)$ is the line shape of the resonance due to Doppler and hyperfine broadening centered at $\nu_r{}^0$ and $S(\nu_\ell - \nu_\ell{}^0)$ is the line shape of the laser centered at $\nu_\ell{}^0$. Γ_T is the line width due to collisions and

natural damping and Γ_e is the contribution to the line width from elastic collisions. In order to evaluate the dependence of $\frac{d\sigma}{d\Omega}$ on pressure, P, and $\Delta\nu = \nu_\ell^0 - \nu_r^0$, we assume that G and S are Gaussians and use Fourier transforms to reduce the double integral to a single integral. We then neglect natural damping, assume the Γ's vary linearly with P, and evaluate the integral numerically as a function of $\Delta\nu$ and P. The results of such a calculation are shown as the curves in Figure 3, where we have assumed that $\Gamma_T = (1.4 \times 10^{-4}\ \text{cm}^{-1}/\text{mm}) \times P$ and that the convoluted Gaussian half width (at 1/e) of the laser and the resonance is 0.024 cm^{-1}. Overall normalization was set by a best fit to the $\Delta\nu = 0$ data. It is clear that this model calculation adequately represents the data as a function of $(\Delta\nu)$ and P.

Resonance Raman Scattering in NO_2

Unlike I_2, the spectroscopy of NO_2 is very poorly understood and one cannot determine a priori the laser frequency which will give the largest resonance enhancements. The absorption spectrum extends from about 2500 to 6500 Å[37] and appears to be a broad continuum with some sharp structure superimposed upon it.[38] Since we expect to find large enhancements associated with sharp absorption lines whose width is of the order of 0.1 Å, a complete investigation of NO_2 at wavelengths longer than its dissociation limit (∿4000 Å) would involve taking spectra at roughly 25,000 laser frequencies. This would be an immense undertaking. Our approach to finding the largest Raman cross section was to concentrate on the ν_2 Raman mode which is located 750 cm^{-1} below the laser frequency and measure its intensity variation as a narrow-band laser (0.1 Å) was continuously scanned through the NO_2 absorption spectrum.

Experimental details. The tunable laser used in these experiments was the same as that used for the iodine experiments. The six dye solutions used to cover the wavelength region from 4235-6025 Å are listed in Table II. The laser bandwidth was narrowed by using an intracavity beam expanding telescope in series with a grating which formed one end mirror of the cavity. The grating was blazed at 61° and operated in fifth or sixth order. In this configuration the laser had a bandwidth of $\sim$0.5 cm^{-1} and could be continuously tuned over the entire gain profile of a single dye by using a small clock motor to drive a micrometer which controlled the grating tilt angle. During such tuning, occasional slight adjustment of the vertical tilt of the grating was necessary to maintain maximum output power. In order to further decrease the line width for higher resolution scanning of a limited region, we used the pressure tuning scheme described previously.

A quantity of purified NO_2 was obtained from Dr. Harold Johnston's group in the Chemistry Department at the University of California, Berkeley. Purification[39] was carried out by first storing liquid N_2O_4 in 1 atm of O_2 at 0°C for 24 hours. The material was then placed in a dry ice bath and uncondensed gas was removed by pumping. The condensate was then distilled from -20°C to -76°C several times, with the first portion of the distillate discarded in an attempt to remove HNO_3. A sample of the resulting gas, at 1 mm pressure, was enclosed in a pyrex cell 4.5 cm in diameter and 5 cm long. Fluorescence from the sample was collected in a direction perpendicular to the incident beam with an f/3.4 lens and focused onto the entrance slit of a Jarrell-Ash double monochromator. In order to avoid heating or dissociation of the NO_2, a cylindrical lens

Table II. Laser dyes used in scans of NO_2 spectrum. Nitrogen laser powers were 20-25 mW during these runs.

DYE	TUNING RANGE(Å)	MAXIMUM POWER DURING SCAN (mW)
Coumarin 120	4235 - 4454	0.5
7 Diethylamino-4 Methyl-Coumarin (7D4MC)	4413 - 4714	1.5
Coumarin 102	4651 - 4935	1.8
50% (7D4MC) + 50% Coumarin 6	5014 - 5307	0.4
Fluorescein Disodium Salt	5357 - 5580	0.4
Rhodamine 6G	5712 - 6025	0.7

was placed before the sample. This lens defocused the incident laser along a line coincident with the axis of the spectrometer, forming a beam about 2 mm × 3 cm at the position of the sample. The incident light was polarized perpendicular to the entrance slit of the monochromator, and no attempt was made to analyze the scattered light. Light reaching the exit slit of the monochromator was detected by a photomultiplier (either RCA 8575 or RCA 7265) whose output passed through a gated integrator (See Section III.) which displayed the results on a chart recorder.

Four types of experiments were performed with the apparatus just described. First, a coarse scan was taken through the gain profiles of the six dyes listed in Table II. For this experiment, the laser did not contain the intracavity etalon, and its frequency was varied by using a clock motor to drive the grating mount. The spectrometer was set to the ν_2 mode of NO_2 at 750 cm^{-1} from the laser frequency and was advanced by hand every time the laser scanned $\sim$7 Å. The bandpass of the spectrometer was 25 Å for these experiments. Any sharp intense structure seen on this first scan was rescanned in the same manner to check reproducibility. In Figure 4 we present the most interesting structures found with this experimental procedure. For a given dye, other structures were observed, but they were either of lower intensity or did not consist of resolved sharp lines. One of the structures shown in Figure 4 occurs in a region described by Douglas and Huber[38] in their study of the NO_2 absorption spectrum, and we chose to investigate this region in more detail. For this purpose, we inserted the intracavity etalon into the laser and, with the spectrometer set 750 cm^{-1} from the central frequency of the band, we

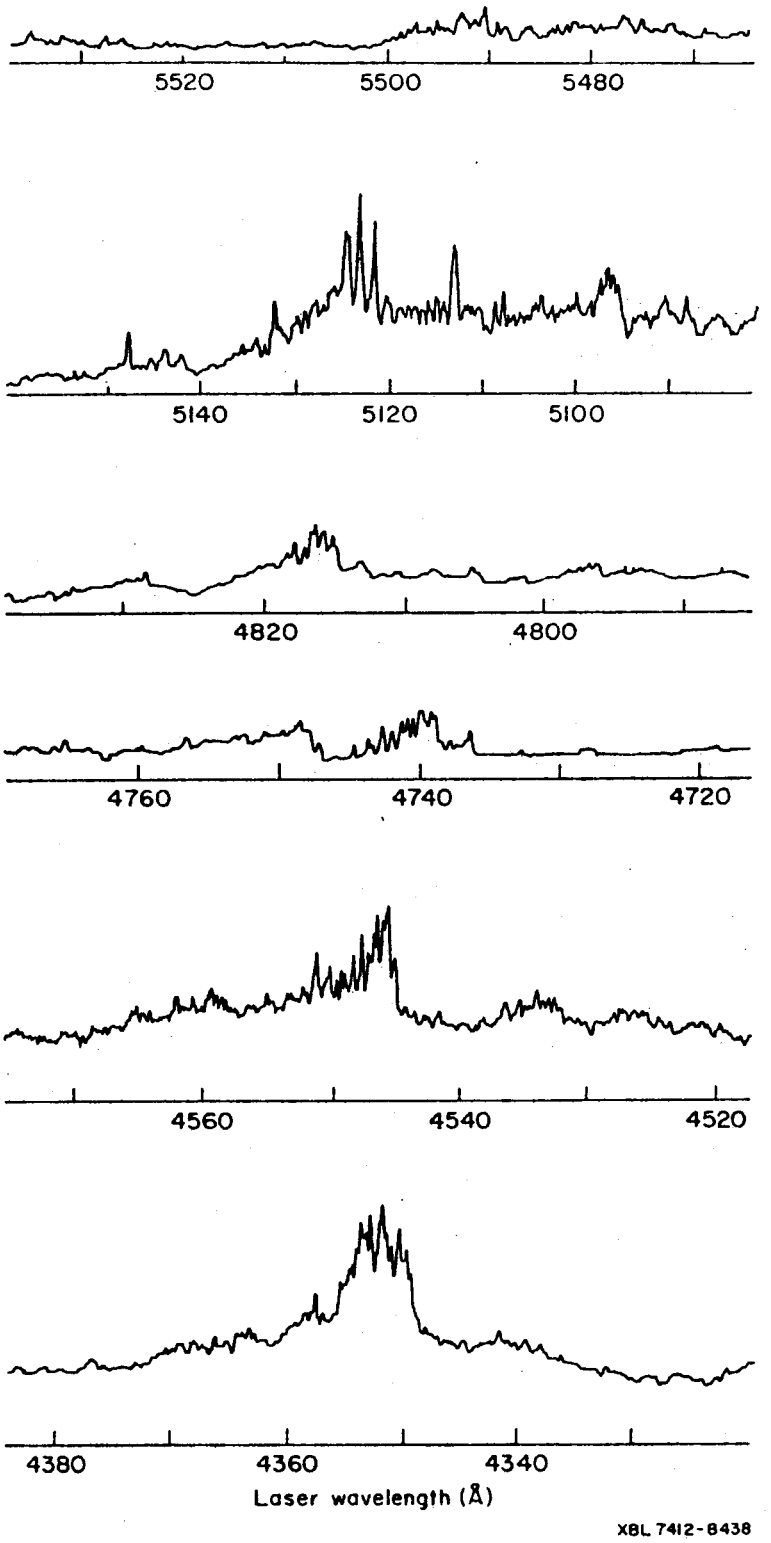

Figure 4. Intensity in the ν_2 mode as a function of laser wavelength over wavelength regions where sharp and intense structures were observed. The bandwidth of the laser was ≈0.1 Å and the spectrometer bandwidth was set to 25 Å. The intensities in different scans cannot be compared directly due to variations in laser power and detector sensitivity.

used our pressure tuning to vary the laser frequency across the band. The result of this scan is shown in Figure 5 where now one can see the individual lines resolved clearly. The spectrometer bandwidth was $\sim$120 cm^{-1} for these experiments. The lines shown can be correlated directly with those seen in absorption by Douglas and Huber.[38]

By scanning the spectrometer with the laser tuned to frequencies near line B in Figure 5, we have taken low resolution spectra of the fluorescence from NO_2. Figure 6 shows scans taken at laser frequency shifts of $\Delta\nu$ = 0, -0.04, and -0.2 cm^{-1} from line B with a spectrometer bandwidth of 120 cm^{-1}. It is apparent that the intensities of the ν_2 mode and its first and second overtones are strongly frequency dependent. Finally, we have made high resolution spectrometer scans of the ν_2 mode with the laser set to the peak frequencies of the strong lines in Figure 5 (designated by the letters A through H). The monochromator bandwidth for these experiments was set to 4 cm^{-1}. Each scan included not only the ν_2 mode, but also a xenon calibration line located at 4697.0 Å. Using this calibration line we could determine the absolute location of the ν_2 mode to $\pm$0.5 cm^{-1}. Some examples of these high resolution spectra are shown in Figure 7. We have made use of the observed splittings of the ν_2 mode to identify the initial, intermediate, and final rotational states for the transitions shown.

Discussion. The visible absoprtion spectrum of NO_2 has a complex structure which has been analyzed only to a limited extent. We have studied the intensity of the ν_2 fluorescence mode throughout most of the visible absorption spectrum and have observed the six intense and sharp structures

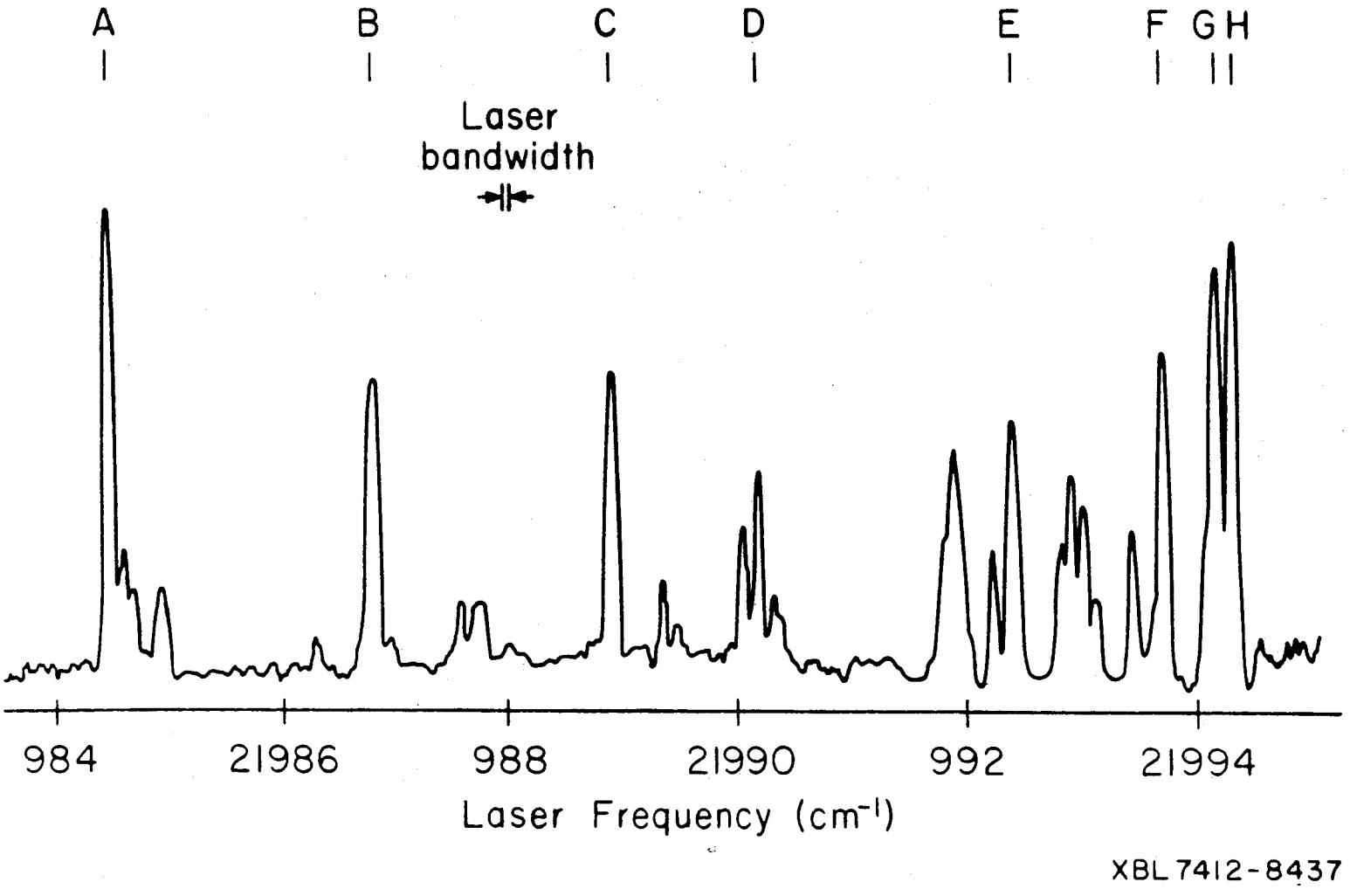

Figure 5. Intensity in the ν_2 mode as a function of laser frequency, near 22,000 cm^{-1} (4545 Å) with narrow-band laser excitation. The line width of the laser was $\sim$0.04 cm^{-1} and the bandwidth of the spectrometer, 120 cm^{-1}. The relative positions of the lines could be determined to ±3%, and the absolute positions were set using the wavelength determination of Douglas and Huber for the A(13) line which corresponds to line B in our scan.

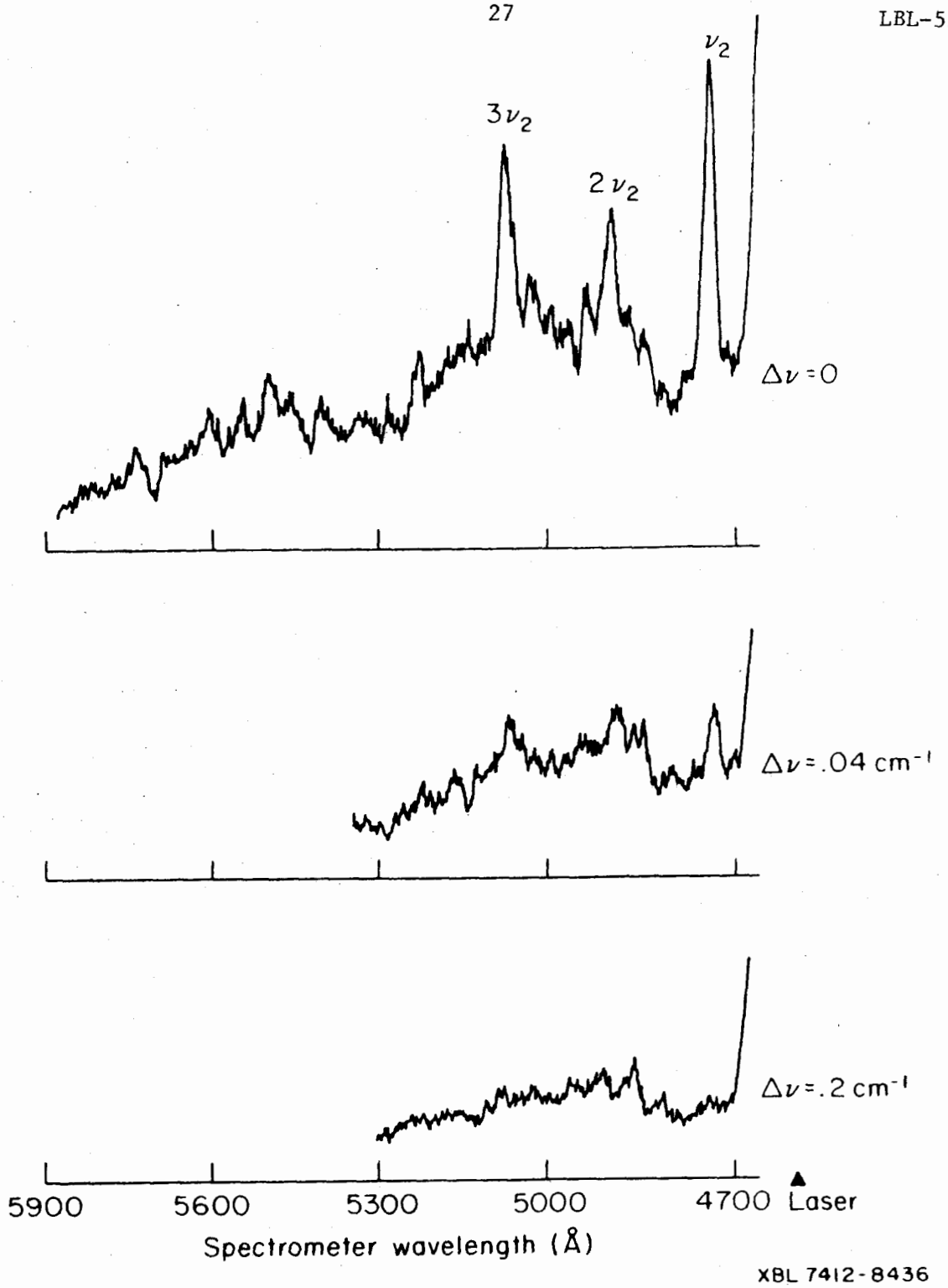

Figure 6. Low resolution scans of the fluorescence taken with laser frequency shifts of 0, -0.04, and -0.2 cm^{-1} from line B of Figure 5. The bandwidth of the spectrometer was 120 cm^{-1} and the laser bandwidth was 0.04 cm^{-1}.

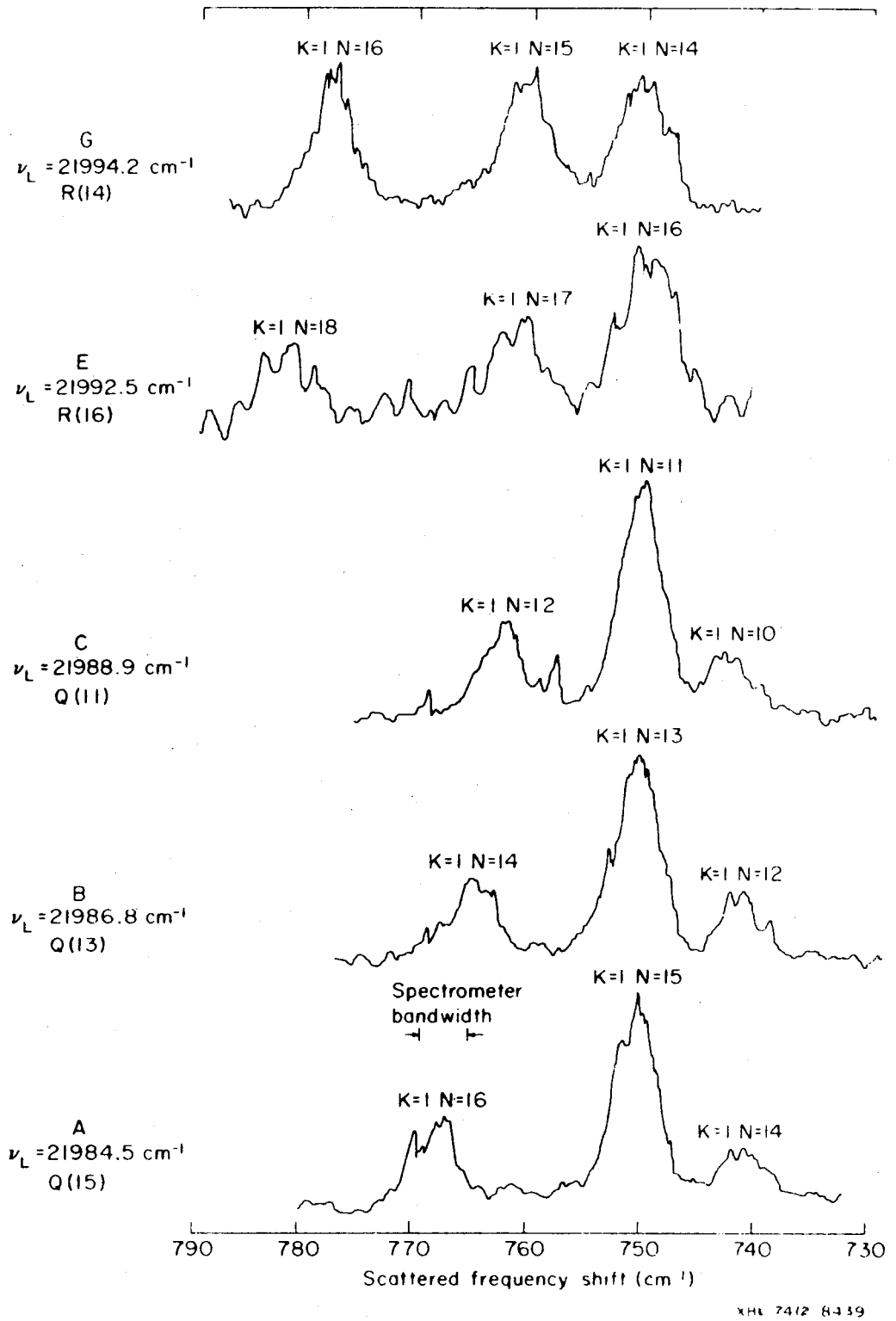

Figure 7. High resolution spectrometer scans of the ν_2 mode located $\sim$750 cm^{-1} lower in frequency than the laser. The laser was tuned to the peaks of lines A, B, C, E, and G of Figure 5. The K and N values refer to the final state of the various transitions. The spectrometer bandwidth was 4 cm^{-1} and the laser bandwidth, 0.04 cm^{-1}.

shown in Figure 4. The positions of five of these structures located at 18,215, 19,523, 21,099, 21,996, and 22,990 cm^{-1} are given to within 10 cm^{-1} by the following formula $\nu = 18{,}215 + 576.22\ N + 36.38\ N^2$ with N respectively equal to 0, 2, 4, 5, 6. The frequencies corresponding to N = 1 and N = 3 occur at gaps between wavelength regions covered by the dyes. We speculate that there may be similar structures corresponding to N = 1 and N = 3, with all seven structures forming a smooth progression. We are uncertain of the explanation for this progression; however, if it is due to vibrational spacing in the upper state, then it has a peculiar anharmonicity, since the spacing between members of the progression increases with frequency. It should be noted that, of the six observed structures, only the one near 4545 Å corresponds to any of the bands reported by Douglas and Huber.[38] With the laser tuned to the peaks of the most intense lines within these structures, we observe fluorescence cross sections into the ν_2 mode which are about 2 orders of magnitude larger than those typically observed using fixed frequency lasers.[40] For example, at the peak of line B in Figure 5 we have measured a cross section of 1.4×10^{-24} cm^2/sr at 1 mm of NO_2 pressure. The large scattering cross sections are particularly surprising given the fact that the absorption cross sections we have measured at lines near 4545 Å are comparable to that of the background absorption. These sharp and intense structures might be due to transitions to intermediate states which are not perturbed by high lying vibrational levels of the ground state.[41] Such an explanation is consistent with the large enhancements we have measured.

We have investigated the band near 4545 Å in much greater detail than

the other bands. As shown in Figure 5, this band has a sharp and complex structure. We have attempted to make a partial rotational analysis of this region by tuning the laser to several of the most intense lines, designated by the letters A through H in Figure 5, and resolving the ν_2 fluorescence mode located[42] at 749.8 cm^{-1}. In Figure 7 the resolved fluorescence for the laser tuned to lines A, B, C, E, and G are presented. Since the narrow band laser selects a single initial to intermediate state transition, the observed triplet structures can be used in combination with the selection rules for a slightly asymmetric top ($\Delta N = \pm 1.0$; $\Delta K = \pm 1.0$) and the ground state spectroscopic constants, to assign the final state quantum numbers. This determination then allows one to make assignments for both the initial and intermediate states.

The rotational energy levels of a slightly asymmetric top can be written approximately as[43]:

$$E(N,K) = \frac{1}{2}(B_o + C_o)N(N+1) + [A_o - \frac{1}{2}(B_o + C_o)](1 - 3/8b^2 - \ldots)K^2 + \Delta B^K_{eff}\, N(N+1) + \Delta D^K_{eff}\, N^2(N+1)^2 + \ldots \quad (5)$$

where N and K are the quantum numbers appropriate in the symmetric top limit. The quantity b is an asymmetry parameter given by:

$$b = \frac{C_o - B_o}{2[A_o - \frac{1}{2}(C_o + B_o)]} . \quad (6)$$

ΔB^K_{eff} and ΔD^K_{eff} are K dependent functions of b which vanish as b goes to zero. The formulae for ΔB^K_{eff} and ΔD^K_{eff} are given in full detail by Herzberg.[43] In Eq. (5) we have neglected the vibrational rotational

interaction since this correction is small[44] for the first excited vibrational state. For NO_2 half of these levels are missing due to nuclear statistics. The oxygen atoms have spin 0 and therefore the total wave function (electronic-vibrational-rotational) must be symmetric under interchange of the oxygen nuclei. In the ground state of NO_2, both the electronic and ν_2 vibrational wave functions are symmetric under interchange of the oxygen atoms (They both have A_1 symmetry.). Therefore, for states in which only the ν_2 vibrational mode is excited, no antisymmetric rotational levels will be found. Using Eq. (5) and the appropriate spectroscopic constants[42] (A_o = 8.0012 cm^{-1}, B_o = 0.43364 cm^{-1}, C_o = 0.41040 cm^{-1}) along with Dennison's rules[45] for determining the symmetry of a rotational level, one can construct the energy level diagram of the ground state. By comparing the spacing of adjacent levels with the observed splittings in the triplet structures shown in Figure 7, one can identify the final state of the transitions. These identifications are shown in Figure 7 and a comparison of calculated and observed splittings is made in Table III. We can now identify the initial state quantum numbers by noting that the displacement of the emission lines from the laser frequency corresponds to the difference in energy between the initial and final vibrational-rotational states. Since the vibrational frequency of the ν_2 mode is 749.8 cm^{-1}, it is easy to see from Figure 7 that the initial states for the transitions A, B, C, E, and G are respectively K"=1 N"=15, K"=1 N"=13, K"=1 N"=11, K"=1 N"=16, and K"=1 N"=14. From the initial and final state N values and the selection rule $\Delta N = \pm 1, 0$ the corresponding intermediate state N values must be N'=15, N'=13, N'=11, N'=17, and N'=15. The observation of only odd N' values suggests that K'=0 and that the

Table III. Comparison of calculated and measured splittings between members of triplet structures shown in Fig. 7.

TRANSITION	FINAL STATE N VALUE	FREQUENCY SHIFT FROM CENTRAL N VALUE (cm^{-1})	
		CALCULATED	MEASURED
	16	16.5	17.5
A	15	-	-
	14	-10.0	- 9.3
	14	14.1	13.8
B	13	-	-
	12	- 9.0	- 8.8
	12	11.8	11.7
C	11	-	-
	10	- 7.9	- 7.2
	18	20.2	19.0
E	17	-	-
	16	-11.3	-11.0
	16	16.5	16.7
G	15	-	-
	14	-10.0	-10.1

intermediate state vibronic wave function is antisymmetric under interchange of the oxygen nuclei. For all other K' values, one would expect to observe both even and odd values of N'.[45] These assignments are consistent with those made by Douglas and Huber[38] from their high resolution absorption measurements. We have also tried to make further assignments by tuning the laser to lines D, F, and H. However, the fluorescence did not show a triplet structure and could not be used for identification.

Fluorescence Lifetimes in NO_2

In collaboration with the Bradley Moore group we have also made measurements of the fluorescence lifetimes at several lines within the sharp structure near 4545 Å. These experiments were motivated by the observation that the fluorescence lifetime of NO_2 is anomalously long when compared to the lifetime obtained from the integrated absorption coefficient. This effect is believed to arise from interactions between the different electronic levels in the visible region. Despite much effort to observe short-lived states directly, only two such observations have been reported to date. The first of these involved $K_a = 0$, $^2B_1$ lines which form prominent features of the absorption spectrum near 4545 Å.[46] Its accuracy was severely limited, however, by poor signal to noise and lack of shot-to-shot stability in the laser employed. The second of these observations[47] involved not the $K_a = 0$, $^2B_1$ lines, but rather a 5_{24}, $^2B_2$ rotational level pumped by the 488-nm line of an argon ion laser. A lifetime of 3.39 ± 0.36 μsec was obtained from the line width of the microwave-optical double resonance signal. In collaboration with Moore's group we have performed an experiment which shows that

$K_a = 0$, $^2B_1$ lines near 4545 Å do not have the short lifetimes expected from previous experimental results and perturbation analysis.

Figure 8 shows the experimental arrangement. A nitrogen-laser-pumped dye laser of 1-GHz bandwidth (Molectron DL-300 pumped by Molectron UV-1000) was used to excite NO_2 in a 22-liter bulb connected to a greaseless vacuum system. Pressures were measured with a capacitance manometer (MKS Baratron, Type 300BH-1 Head). The laser frequency was scanned (Molectron Scanning Unit Model DL-404B), and fluorescence at right angles to the beam was observed by two photomultipliers. One photomultiplier (EMI 9659B, PM-1) was equipped with a blue cutoff filter (Schott RG-530) and observed "red" fluorescence with $\lambda_{fluor} > 530$ nm. The second photomultiplier (RCA 8575, PM-2) observed fluorescence which was focused using f/10 optics and resolved by a monochromator (Spex, 3/4 m). The monochromator was set to pass "blue" fluorescence 750 cm^{-1} below the excitation line with a bandpass of roughly 90 cm^{-1} (FWHM, 2-mm slits).

At specific lines in the excitation spectrum, the laser scan was stopped and the lifetime measurements were made using the 22-liter bulb for both the red and the blue fluorescence. To obtain improved signal to noise, many fluorescence traces were digitized (Biomation 8100 Transient Recorder) and averaged (Northern 575 Signal Averager). During the period in which the fluorescence was averaged, typically 2-5 min, the laser remained stable in frequency to $\sim$1 GHz as judged by the signal intensity of the excitation spectrum.

Fluorescence in either the blue or red region appeared to decay with a single exponential. Reciprocal lifetimes as a function of pressure are shown in Figure 9 both for the red fluorescence and for the blue

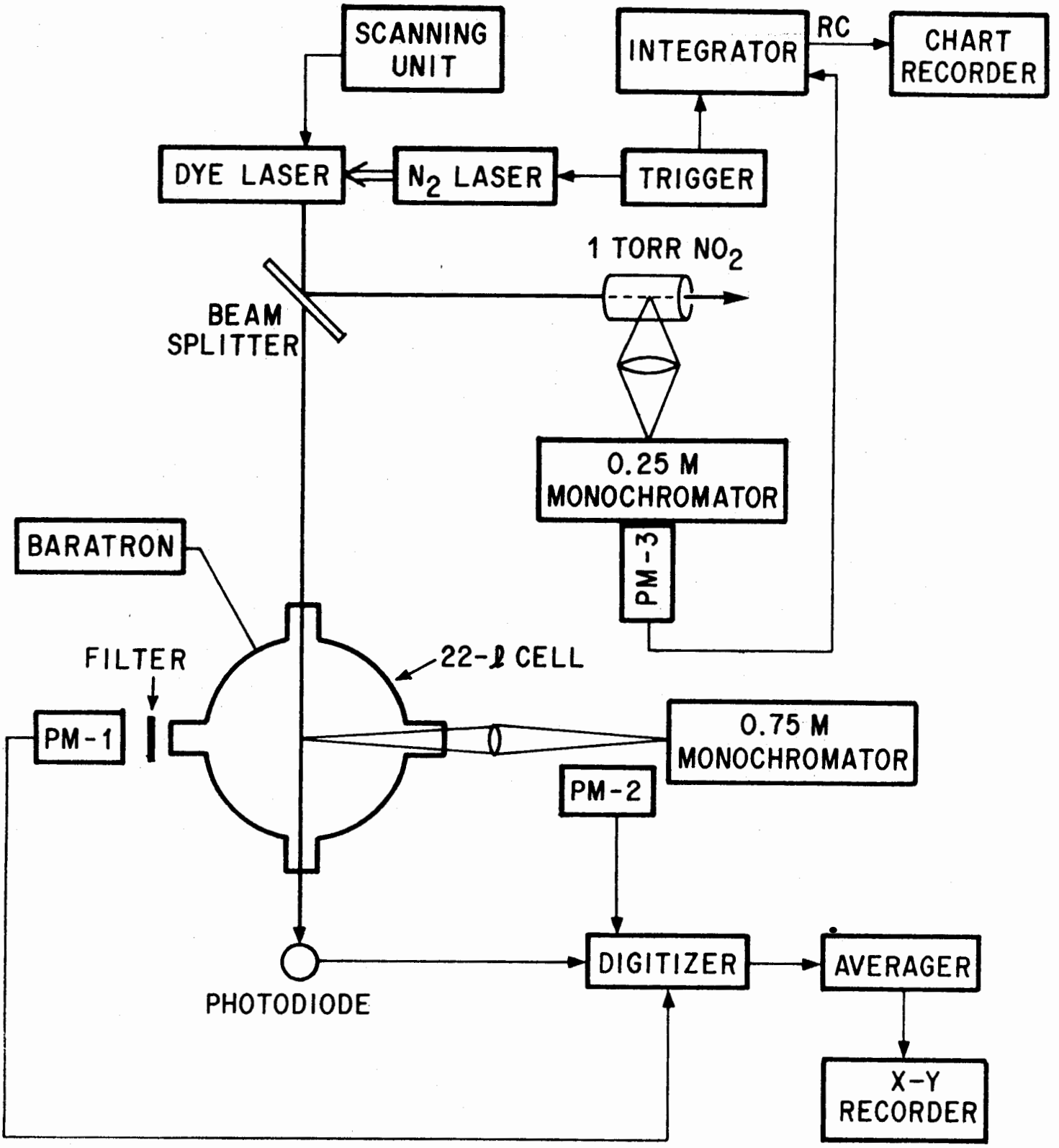

XBL 755-1358

Figure 8. Experimental apparatus for recording the fluorescence excitation spectrum and measuring the lifetimes of NO_2.

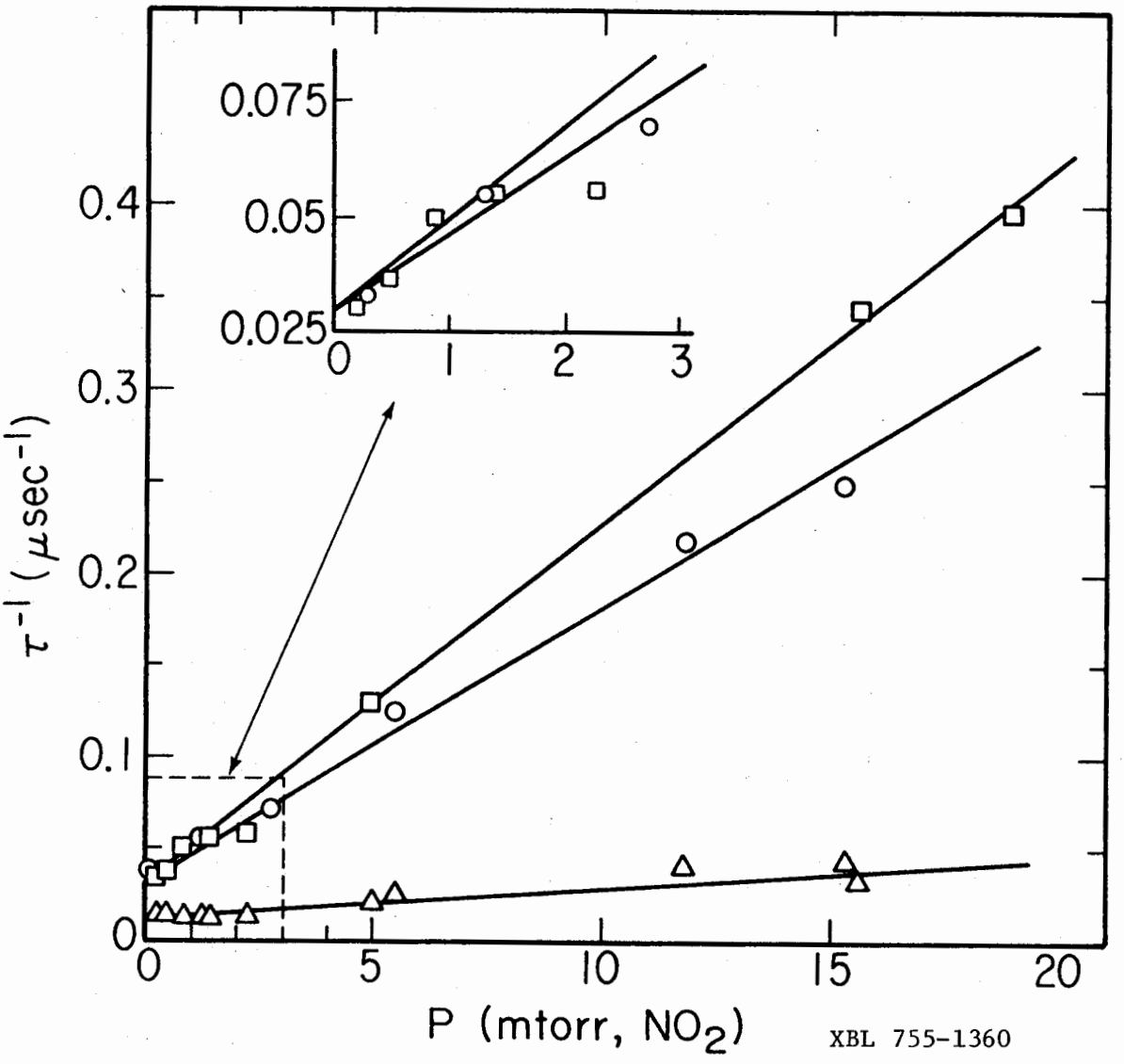

Figure 9. Reciprocal lifetimes for NO_2 fluorescence as a function of pressure. The circles and squares are for resolved blue fluorescence excited by the Q(13) and Q(11) lines, respectively. The triangles are for the unresolved red fluorescence. The insert shows an expansion of the low-pressure region for the blue fluorescence.

fluorescence excited at each of the Q(11) and Q(13) lines denoted by B and C in Figure 5.

The zero-pressure lifetime of the blue fluorescence excited by either the Q(11) or Q(13) lines is found to be 33 ± 4 μsec. A careful examination of the low-pressure fluorescence traces for fast components with lifetimes on the order of 1-3 μsec has shown that such components, if present, form less than 5% of the fluorescence amplitude. Previous investigators have found short components for $K_a = 0$ states whose amplitude at unspecified pressures was roughly 13% of the broad band fluorescence. Since our experiment isolates fluorescence specifically from $K_a = 0$ states, it should be extremely sensitive to such short components if present. Since no evidence for these components was found, we conclude that $K_a = 0$ lines of the $^2B_1$ electronic state do not have short lifetimes comparable to the integrated absorption lifetime of 0.3 μsec. This fact may indicate that such lines are still appreciably perturbed. However, the fact that these states do stand out in the absorption spectrum and even more so in the excitation spectrum of the ν_2 fluorescence mode suggests that they are unperturbed. Since a lengthening of the lifetime by a factor of 100 is not compatible with unperturbed states, perhaps the oscillator intensity from which a 0.3 μsec lifetime is deduced may be that of the $^2B_2$ state. If, in fact, the $K_a = 0$ levels are unperturbed, then the lifetime measured in this experiment may be the true lifetime of the $^2B_1$ electronic state.

SECTION III

SPINOFF RESEARCH

During the course of this project we have made some progress in scientific areas not directly related to the initial goals of the proposal. These include some preliminary experiments on using modulated fluorescence as a monitor for ambient NO_2 levels and the development and construction of an inexpensive analog gate used for detecting small signal levels from a photomultiplier. Also, one of the authors (H.R.) has collaborated with T. Novakov to explore the feasibility of using Raman scattering for characterizing ambient aerosols. These areas of research will be described in this section of the report.

Modulated Fluorescence as a Possible In-situ Monitor for NO_2

Recently, Tucker et al.[48] have reported the successful operation of an ambient NO_2 monitor based on laser excited broad band molecular fluorescence. In order to avoid fluorescence from aerosols, however, it was necessary to filter the incoming air stream. This filtering procedure could change the measured NO_2 concentration either because of adsorption directly on the filter or on particulates trapped by the filter. We have investigated an alternate procedure which has the virtue that it requires no processing of the air sample and can monitor NO_2 and particulates simultaneously.

In our work on the excitation spectrum of the ν_2 fluorescence mode of NO_2 described in Section II, we found several narrow spectral regions in which this reemission mode is sharply enhanced. Following the work of Tucker et al.,[48] we have looked at broad band fluorescence from 1 mm of NO_2 in 1 atm of N_2 as we tuned a laser over some of the sharp excitation

lines which were found in our earlier study. We find substantial modulation of the broad band fluorescence. This modulation occurs when the laser is tuned over a very narrow spectral region and is characteristic of NO_2. Since particulate fluorescence is expected to change quite slowly with laser frequency, we feel that we have found the basis for an ideal way to separate NO_2 fluorescence from particulate fluorescence.

The laser used in this experiment was in the same configuration as that used for the iodine experiments. Using a 5×10^{-3} molar solution of 7D4MC in ethanol as a dye, the laser had a bandwidth of 0.04 cm^{-1} and an average power of 0.15 mW near 4545 Å. The laser beam was directed along the axis of a quartz cell 5 cm in diameter and 60 cm long which had Suprasil entrance and exit windows. The exit window was set at Brewster's angle to prevent the beam from being reflected back through the cell. The beam, after passing through the cell, was dumped in a beam absorber similar to that described in Tucker et al.[48] The cell was filled with 1 mm of NO_2 and 1 atm of N_2. Fluorescence from this sample was observed at right angles to the beam direction by an RCA 7265 photomultiplier located at the midpoint of the quartz cell. A liquid filter of $Na_2Cr_2O_7$ in distilled water (304 g/liter) was placed in front of the photomultiplier to eliminate background at the laser frequency. Several baffles were inserted in the cell to prevent the detector from directly viewing the windows of the cell.

We have observed the broad band fluorescence as we tuned the laser over the lines designated by A, B, and C in Figure 5. Figure 10a shows the behavior of this fluorescence as a function of laser frequency and compares it with the ν_2 excitation spectrum of 1 mm of NO_2 in vacuum

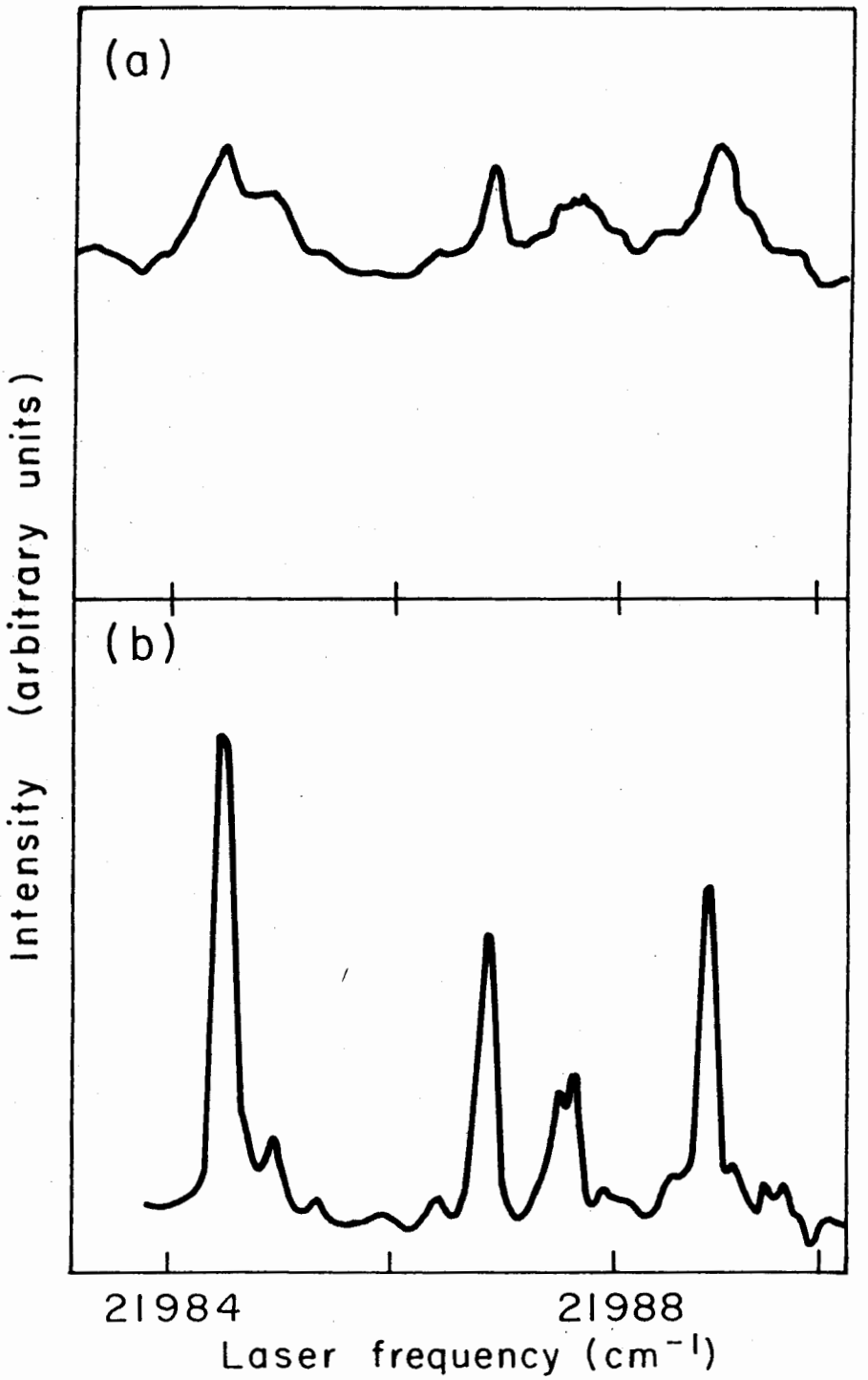

XBL 7511-9531

Figure 10. a) Intensity of broad band fluorescence of 1 mm of NO_2 in 1 atm of N_2 as a function of laser frequency. b) Intensity of ν_2 fluorescence for 1 mm of NO_2 as a function of laser frequency.

shown in Figure 10b. The figure clearly shows modulation of the broad band fluorescence as the laser is tuned over these sharp transitions. A background check with the cell filled with 1 atm of N_2 gave a signal <1% of the signal shown in Figure 10a. The modulation which we have observed is large enough to allow one to use it easily to separate aerosol fluorescence from that of NO_2 in ambient air provided that the signal from aerosols is comparable to that from NO_2 and there is little additional background in the measuring apparatus. Gelbwachs and Birnbaum[24] have shown that, at least for some spectral regions, the aerosol fluorescence and that of NO_2 are comparable in intensity, and Tucker et al.[48] have operated an apparatus which has very low background fluorescence. Our measurements therefore show that the use of a tunable source may allow measurement of both aerosols and NO_2 simultaneously at ambient levels with no processing of the polluted air.

Design of a Simple and Inexpensive Analog Gate

Pulsed lasers are often used as light sources for Raman scattering, fluorescence, luminescence, and absorption studies. Since the duty cycle of these sources is usually very poor, one would like to design detection electronics which are sensitive for only a small time interval around the laser pulse in order to improve signal to noise. For example, if one uses a nitrogen-laser-pumped dye laser, its output might typically consist of 5 nsec pulses at a repetition rate of 10 Hz. The rise times of typical photomultipliers are a few nanoseconds; therefore, except at very low light levels ($\gtrsim$1 photoelectron/pulse), one cannot use photon counting techniques, since the photoelectron pulses will, in general,

pile up. It is therefore necessary to integrate the charge from the photomultiplier. In the absence of a gating scheme, even a low-noise, high-gain tube, such as an RCA 8575, contributes a background noise equivalent to about 10^4 photoelectrons/sec. It is apparent that even a rather slow gate will improve things significantly. For example, a 10-μsec gate operating at 10 Hz will reduce the background level to 1 photoelectron/sec.

We have designed and built a simple and inexpensive analog gate which is used in combination with an electrometer operating as a ratemeter. The output of the ratemeter is displayed on a chart recorder. This detection scheme has a sensitivity of better than 1 photoelectron/sec and a linearity of better than 10% over a dynamic range of 10^3. Also, since the electronics are charge sensitive, they are rather insensitive to the large burst of rf noise generated from the pulsed laser source. A schematic of the gate is shown in Figure 11. The input signal is taken directly from the unterminated anode of a photomultiplier and the gate output is fed into an electrometer. The heart of the gate is a low leakage Siliconix 2N4117A FET, which has a gate reverse current of $\leq$1 pA. When the gate is in its quiescent state, the 2N4117A is nonconductive, while the 2N5461 FET conducts any charge appearing on the input line to ground. When a gating pulse occurs (0 to +5 TTL), the 74121 one-shot produces a 15-μsec pulse. This pulse, after going through appropriate shaping circuitry, turns off the 2N5461 FET and turns on the 2N4117A FET, so that charge can pass to the electrometer. Unfortunately, the gating pulse is also capacitively coupled to the input line, allowing some spurious charge to reach the electrometer. We have been able to cancel

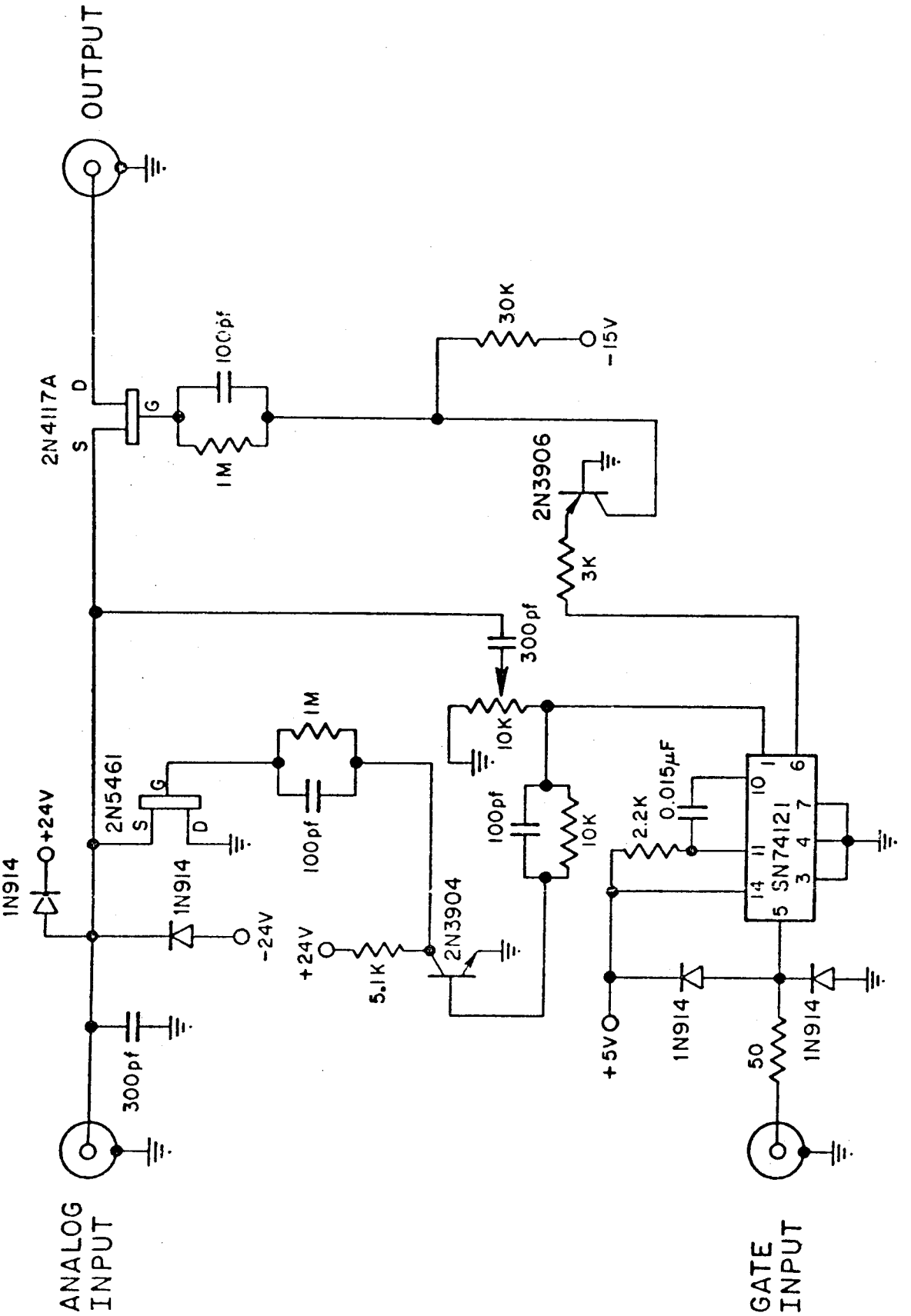

Figure 11. Schematic of analog gate.

this spurious signal effectively by connecting a 300-pF capacitor to the input line and applying an adjustable voltage pulse to it. The zero obtained in this manner drifts slowly in time. With a gain of 10^8 in the photomultiplier, the drift, at the end of 1 hr, corresponds to a spurious signal of about 2 photoelectrons/sec. The diodes connected to the input line serve to protect the 2N4117A FET from large input signals.

Figure 12 shows a typical resonance Raman spectrum of NO_2 taken using our gate and an E-H Research Laboratories model 215 electrometer. The electrometer time constant was 1 sec. The laser used to obtain this spectrum was a nitrogen-laser-pumped dye laser with 0.2 mW of average power. The scattered light passed through a Jarrell-Ash double monochromator and was detected by an RCA 8575 photomultiplier operated at 2500 V. The most intense line in the spectrum corresponds to a signal of about 100 photoelectrons/sec and the background noise level is about ±2 photoelectrons/sec. This scan took about 1 hr to complete and during its course, the baseline shift was less than the noise in the signal. The signal to noise in this spectrum is excellent, but it can be improved further by using larger time constants.

This analog gate may be built from parts costing approximately $20.00. It has excellent sensitivity, good dynamic range, and operates reliably in a high-rf-noise environment. It can be used for any experiment with pulsed light sources in which one wants to measure a small pulsed signal in the presence of a large dc photoelectron background.

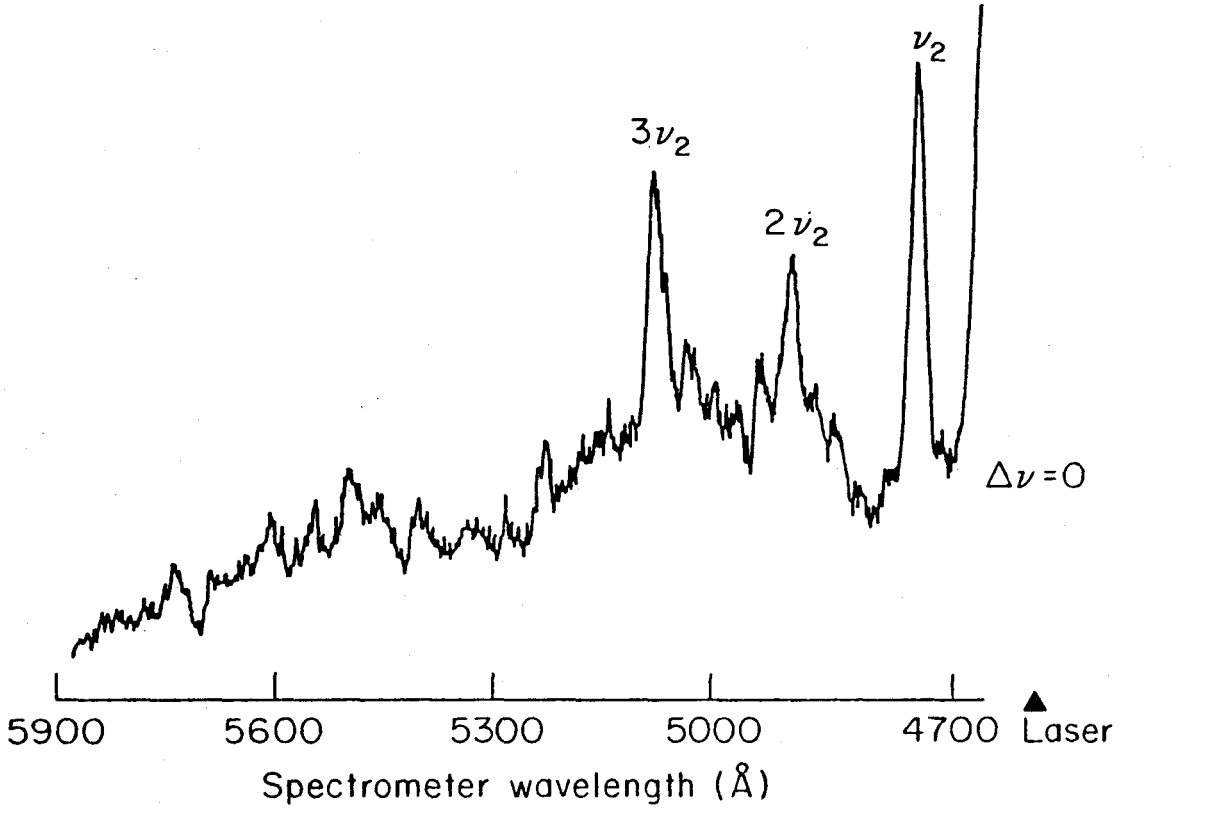

Figure 12. Resonance Raman spectrum of NO_2 taken with our analog gate in combination with an E-H Research Laboratory Model 215 electrometer and an RCA 8575 photomultiplier operated at 2500 V. The time constant of the electrometer was 1 sec and the dye laser average power was 0.2 mW.

Application of Raman Scattering to the Characterization of Atmospheric Aerosol Particles

Airborne particulates play a major role in the air pollution problem. They are responsible for acid rain, reduced visibility, and, in certain size ranges, are deposited in the lungs where they can cause a variety of adverse health effects. Considerable effort has been expended in the analysis of these particulates. Such techniques as wet chemistry, X-ray fluorescence, infrared spectroscopy, and ESCA have been used rather extensively. Yet there are still great uncertainties as to the chemical form and origin of many of the particulate species. In collaboration with T. Novakov, H.R. has engaged in some preliminary studies to explore the feasibility of characterizing particulate pollutants by means of Raman spectroscopy. We believe that this is the first attempt to apply this spectroscopic technique in this area of research. The samples studied were, among others, diesel exhaust particles, automobile exhaust particles (unleaded fuel, no catalytic converter), and several ambient air samples. The spectra from these samples were compared to those of polycrystalline graphite and activated carbon which were used as references. Our results indicate that physical structures similar to activated carbon are a major species and may be the dominant species in both source-enriched and ambient samples. The implications of this observation could be quite important in terms of atmospheric chemistry, health effects, weather modifications, and the effects of aerosols on the albedo.

The experimental setup included a Coherent Radiation argon ion laser operating with 1 W of power at 5145 Å. The laser beam was focused by a 75-mm focal length cylindrical lens to a spot 0.06 mm × 2 mm on the

sample surface, and the backscattered radiation was collected and imaged by an f/3.4 lens onto the slit of a Jarrell Ashe double monochrometer. The incident polarization of the laser was perpendicular to the slit of the spectrometer, and no analysis of the scattered polarization was made. The output of the spectrometer was detected by an FW130 photomultiplier cooled to -20°C and used in a photon-counting mode. The photon pulses, after appropriate pulse shaping, were counted and displayed on a multi-channel analyzer. In order to minimize heating effects, the highly absorbing samples used in these experiments were rotated at 1800 rpm by a motor. In this way one can increase the area illuminated by the laser beam by a large factor with almost no loss in signal level. The focal spot of the laser was located approximately 5 mm below the axis of rotation so that the effective illuminated area was an annulus of radius 5 mm and width 2 mm which yielded a rather low power density of $\sim$1.5 W/cm^2.

The samples used in these experiments were EDM 3 grade polycrystalline graphite obtained from POCO Graphite, Inc., NORIT A activated carbon obtained from Pfanstiehl Labs, diesel exhaust collected on a glass fiber filter, automobile exhaust collected on a glass fiber filter from a number of cold starts of a poorly tuned 1974 Pinto, and an ambient sample collected in 1975 as part of EPA's RAPS program in St. Louis, Missouri. The latter sample was collected on a 1.2-μ millipore filter using a dichotomous sampler[49] and was in the small size range fraction. The diesel and car exhaust samples were removed from the filter and transferred to an aluminum flat. This technique allowed one to obtain excellent Raman spectra of the particulates without interference from the large fluorescence of the filter material. This technique could not be applied to the ambient sample

because of insufficient loading, and therefore in this case the Raman spectrum was obtained directly from the particles on the millipore filter substrate.

In Figure 13 we show the Raman spectrum obtained from automobile exhaust. Similar spectra were observed for diesel exhaust, activated carbon, and polycrystalline graphite with the dominant features of the spectrum occurring between 1200-1700 cm^{-1}. For polycrystalline graphite a strong line is also observed at $\sim$2700 cm^{-1} which we associate with a C-H vibration. In the ambient sample, where the signal to noise is severely limited by the large fluorescence background, the only lines that were clearly seen above the noise level were also in the 1200-1700 cm^{-1} spectral region. In Figure 14 we show the Raman spectrum for the various samples in this region.

Koenig et al.[50] have measured the Raman spectrum of a single crystal of graphite as well as that of polycrystalline graphite and activated carbon. In a single crystal only the Raman mode near 1600 cm^{-1} is observed, and from a group theoretical analysis, it has been assigned to the k = 0 E_{2g} phonons of the graphite lattice. The mode near 1350 cm^{-1} appears only in samples which are not perfectly ordered, and its intensity relative to the one near 1600 cm^{-1} varies inversely with the crystallite size, L_a, as obtained from X-ray data. More recently, Solin et al.[51] have shown that this ratio tends to saturate for crystallite sizes less than 40 Å. The identification of the 1350 cm^{-1} mode is uncertain, but Koenig et al. suggest that it may be due to an A_{1g} phonon which is normally Raman inactive but is active in this case due to a breakdown of the k selection rules by the small crystallites in the sample.

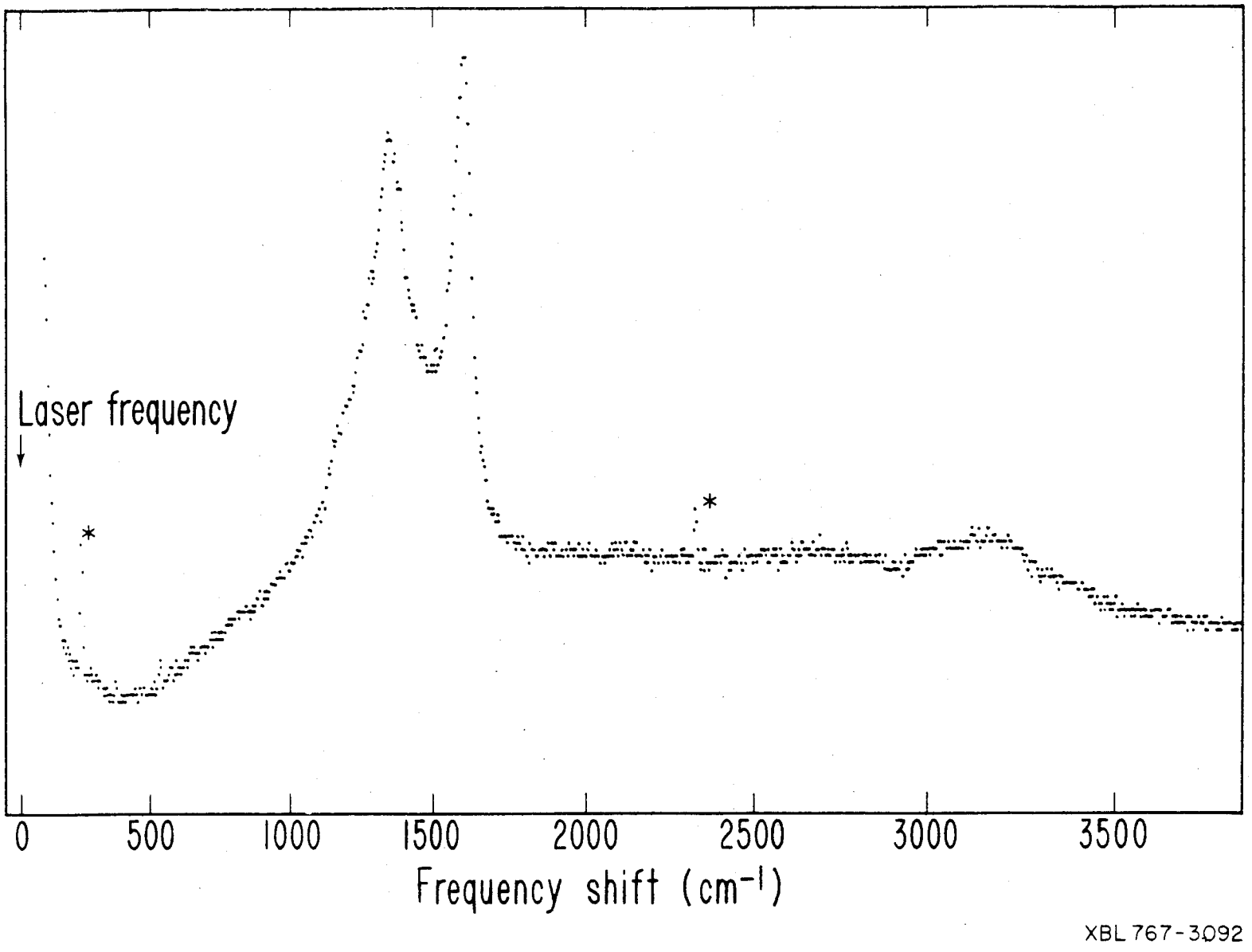

Figure 13. Raman spectrum of automobile exhaust in the spectral region between 90 and 3830 cm^{-1}. The sample was collected from a number of cold starts of a poorly tuned 1974 Pinto using lead-free gas and having no catalytic converter. The slit width for this scan was 3 Å. The lines identified with an asterisk are due to grating ghosts.

Figure 14. Raman spectra between 1200 and 1700 cm^{-1} of:
a) Ambient sample collected in 1975 as part of EPA's RAPS program. The sample was collected on a dichotomous sampler and was in the small size range fraction.
b) Automobile exhaust collected from a number of cold starts of a poorly tuned 1974 Pinto using lead-free gas and having no catalytic converter.
c) Diesel exhaust.
d) Activated carbon.
e) Polycrystalline graphite.
The slit width for samples b-e was 3 Å; while for sample a, 7-Å slit were used to improve signal to noise.

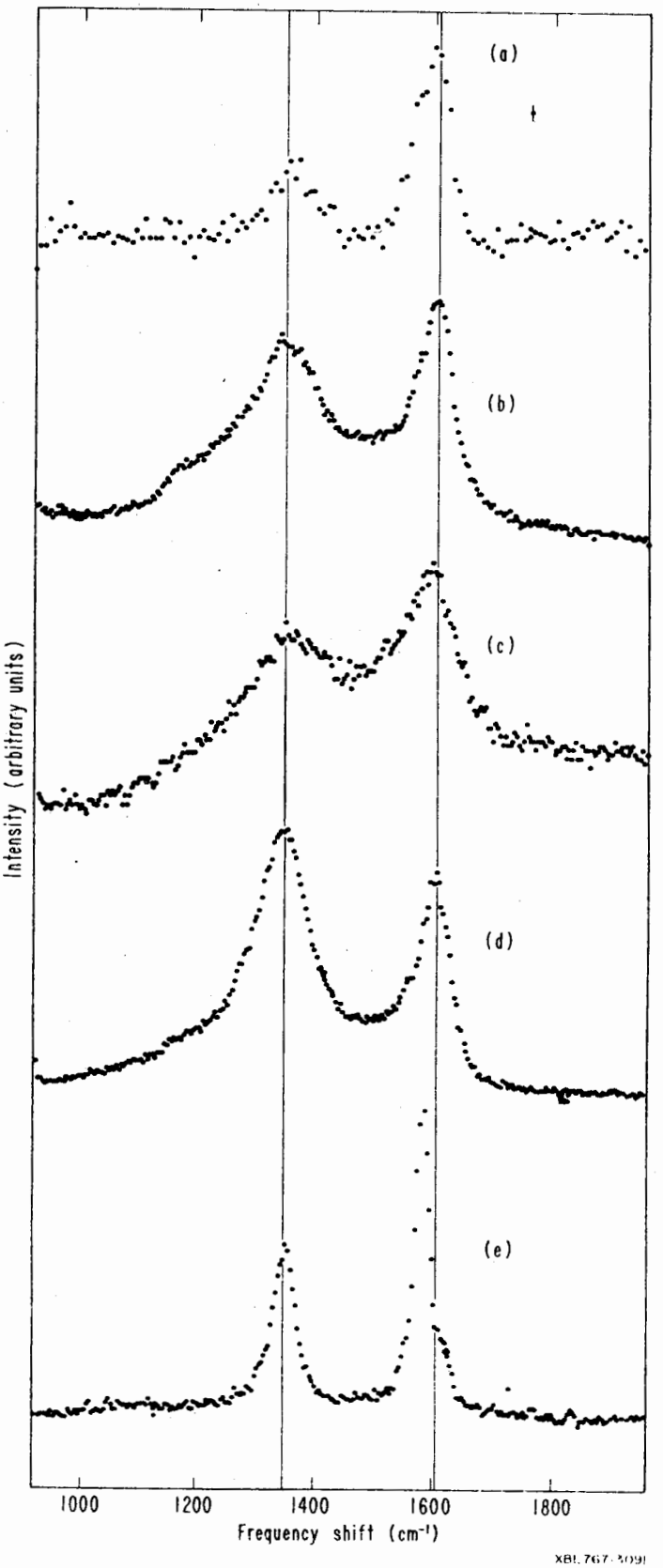

It is evident from Figure 14 that the spectra of activated carbon, diesel exhaust, automobile exhaust, and the ambient sample are very similar. The positions of the two Raman modes in these spectra are coincident to within ±10 cm^{-1} which is the estimated experimental error. Since the phonon frequencies are a sensitive probe of the lattice, we suggest that these spectra give strong evidence for the existence of physical structures similar to activated carbon in the samples we have studied. This is not surprising since activated carbon is also produced in a combustion process.

Using the available results from the literature,[50] we can estimate the crystallite sizes in the various samples from the intensity ratios of the two observed Raman modes. The automobile exhaust and diesel exhaust samples have roughly the same peak intensity ratio, yielding crystallites of ≃50 Å in size, while the ambient sample appears to have crystallite sizes of ≃100 Å. We would expect such structures to have very large internal surface area.

Novakov et al.[52] have recently proposed that fine soot particles, which in many ways are similar to activated carbon, may play a major role in atmospheric chemistry. In order to assess the importance of the proposed soot-catalyzed reactions, it is important to determine the chemically active primary carbon in the carbonaceous fraction of ambient and source-enriched aerosol particles. Our results indicate that physical structures similar to activated carbon are present in diesel exhaust, automobile exhaust, and ambient samples. The fact that these features tend to dominate the Raman spectrum may indicate that graphitic "soot" is the primary species in the samples we have measured. However, the large intensity in

these modes may be due just to their large Raman cross section, and therefore a quantitative interpretation of these results will have to await a more detailed analysis. Such an analysis will have to include measurements of the Raman cross section, optical absorption cross section, and take into account the little-understood particle size effects.

SUMMARY

Although our main conclusions are contained in Section I, we felt it would be useful to present a further qualitative description of the consequences of our study.

The model calculations described in Section I imply that a Lidar system based on the resonance Raman effect and constrained by strict eye safety standards offers little hope for ambient monitoring of gaseous pollutants at distances of the order of one kilometer. If the safety standards could be exceeded by a factor of 10^3 (for example, by using radar to insure that no aircraft were in the field of view), then this conclusion would warrant reevaluation. There would still be the technological problem of making a tunable laser that gives short pulses but has an average power approaching 10 W in the UV. Nighttime monitoring should be easier than daytime monitoring for cases in which wavelengths longer than 3000 Å are involved. Figure 1 indicates the extent of the difference.

For smoke stack monitoring at distances of several hundred meters this method looks competitive with other techniques (ordinary Raman scattering and differential absorption). The sensitivity and selectivity offered by resonance Raman scattering are sufficiently superior to mitigate the technological problems of implementing the scheme.

One general point which becomes clear from our studies of molecular spectroscopy is that it is difficult to make a priori rules for the sensitivity of this technique for various kinds of molecules. One needs

specific spectroscopic information in order to make a reasonable calculation. This information is only available for a limited number of molecules. Our consideration of diatomic molecules indicates that for excitation in a convenient region of the spectrum the cross sections vary by 11 orders of magnitude; therefore, the detection sensitivities vary by a comparable amount, and a decision as to whether resonance Raman scattering is a practical tool for monitoring a given molecule must be made on a case-by-case basis. It seems qualitatively reasonable that more complicated molecules will generally have smaller cross sections, but, as Table I shows, that rule is too simplistic.

For laboratory detection of trace pollutants, where discrimination against the sky light background is not a problem, the preliminary work we have done using modulated broad band fluorescence in NO_2 looks promising. This technique involves tuning a laser over characteristic sharp absorption lines of the molecule and monitoring the broad band fluorescence. The change, or modulation, in intensity of this fluorescence with changing laser frequency allows one to identify the molecule and determine its concentration. Because one measures a scattered signal rather than a small change in a large transmitted signal, this technique seems to offer an attractive alternative to absorption spectroscopy. Since the use of modulation allows one to distinguish one fluorescing species in the presence of others, one need not process the air to remove interference from competing fluorescent sources, such as particulates. Thus this technique seems to offer the opportunity of avoiding any chemical changes that might occur as a result of a filtering process on air samples.

Finally, it seems to us that while tunable lasers do not offer the requisite sensitivity for remote ambient monitoring, they do offer considerable promise for making in situ measurements of ambient samples. The importance of such measurements should be emphasized since there is some uncertainty as to whether monitors which rely on filtering and processing of a sample during its collection do not suffer from bias.

REFERENCES

1. D.A. Leonard, Nature 216, 142 (1967); J.A. Cooney, Appl. Phys. Lett. 12, 40 (1968); T. Kobayasi and H. Inaba, Proc. I.E.E.E. 58, 1968 (1970); S.H. Melfi, J.K. Lawrence, Jr., and M.P. McCormick, Appl. Phys. Lett. 15, 295 (1969).

2. S. Nakahara, K. Ito, S. Ito, A. Fuke, S. Komatsu, H. Inaba, and T. Kobayasi, Opto-electronics 4, 169 (1972).

3. S.H. Melfi, M.L. Brumfield, and R.W. Storey, Jr., Appl. Phys. Lett. 22, 402 (1973).

4. T. Hirschfeld, E.R. Schildkraut, H. Tannenbaum, and D. Tannenbaum, Appl. Phys. Lett. 22, 38 (1973).

5. There has been considerable confusion in the use of the terms Raman scattering, resonance Raman scattering and fluorescence. We are concerned with a scattering process in which the energy difference between the initial and final state photon corresponds to the energy difference between the initial and final states of the molecule. Throughout this report we adopt the point of view that in this case, there is no fundamental distinction between fluorescence and Raman scattering. We, therefore, use the term Raman scattering for the process; and when the laser is near or on a resonance, we use resonance Raman scattering.

6. C.M. Penney, W.W. Morey, R.L. St. Peters, S.D. Silverstein, M. Lapp, and D.R. White, N.A.S.A. Report Number NASA-CR-132363.

7. We should point out that in this case the inelastic scattering is not Raman scattering since the excitation is at the 0-1 vibrational transition and the reemission process occurs after vibrational relaxation at the 0-0 transition.

8. F.L. Baardsen and R.W. Terhune, Appl. Phys. Lett. 21, 209 (1972).

9. C.C. Wang and L.I. Davis, Phys. Rev. Lett. 32, 349 (1974).

10. D.L. Huber, Phys. Rev. 178, 93 (1969); R.L. St. Peters and S.D. Silverstein, Optics Commun. 7, 193 (1973).

11. We should note that operating at the peak of the resonance should not cause a time delay problem in a Lidar system since the lifetime of the intermediate state at atmospheric pressure is of the order of 0.1 nsec.

12. "The Band Spectrum of Carbon Monoxide," National Bureau of Standards Reference Data Series, National Bureau of Standards #5.

13. W.H. Smith, Astro. Phys. J. 176, 265 (1972).

14. J. Anketell and Anne Pery-Thorne, Proc. Royal Soc. A 301, 343 (1967).

15. W.R. Jarmain, P.A. Fraser, and R.W. Nicholls, Astro. Phys. J. 122, 55 (1955).

16. A.J.D. Farmer, V. Hasson, and R.W. Nicholls, J. Quant. Spectrosc. and Radiat. Transfer 12, 627 (1972).

17. H.A. Ory, A.G. Gittleman, and J.P. Maddox, Astro. Phys. J. 139, 346 (1964).

18. J. Tellinghuisen, J. Chem. Phys. 58, 2821 (1973).

19. The Franck-Condon factors were obtained from J. Tellinghuisen in a private communication.

20. J.A. Coxon, specialist periodical report on electronic spectroscopy prepared for the Chem. Soc. of London edited by R.F. Barrow.

21. J.A. Coxon, J. Quant. Spectrosc. and Radiat. Transfer 12, 639 (1972).

22. J.A. Coxon, J. Quant. Spectrosc. and Radiat. Transfer 11, 1355 (1971).

23. G. Herzberg, Spectra of Diatomic Molecules (Van Nostrand Reinhold, New York, 1950), p. 124.

24. J. Gelbwachs and M. Birnbaum, Appl. Optics 12, 2442 (1973).

25. ANSI Z136.1 Laser Safety Standards (1973).

26. W.A. Baum and L. Dunkelman, J. Opt. Soc. Am. 45, 166 (1955).

27. G.L. Knestrick and J.A. Curcio, Appl. Optics 6, 2105 (1967) and Appl. Optics 9, 1574 (1970).

28. For example, there is a commercial system made by Molectron which gives >0.5 mJ/pulse at 25 Hz throughout the visible.

29. F.B. Dunning, E.D. Stokes, R.F. Stebbings, Opt. Comm. 6, 63 (1973); F.B. Dunning, F.K. Tittel, R.F. Stebbings, Opt. Comm. 7, 181 (1972).

30. C.F. Dewey, Jr., W.R. Cook, Jr., R.T. Hodgson, J.J. Wynne, VIII International Quantum Electronics Conference, San Francisco, July 1974; C.F. Dewey, W.R. Cook, R.T. Hodgson, and J.J. Wynne (to be published).

31. A.G. Massey, VIII International Quantum Electronics Conference, San Francisco, July 1974.

32. D.G. Fouche and R.K. Chang, Phys. Rev. Lett. 29, 536 (1972); R.L. St. Peters, S.D. Silverstein, M. Lapp, and C.M. Penny, Phys. Rev. Lett. 30, 191 (1973).

33. T.W. Hänsch, Appl. Optics 11, 895 (1972).

34. The most intense peaks were identified using the analysis of R.F. Barrow and K.K. Yee, J. Chem. Soc. Faraday Trans. II 69, 684 (1973).

35. D.G. Fouche and R.K. Chang, App. Phys. Lett. 20, 256 (1972).

36. J.G. Skinner and W.G. Nilsen, J. Opt. Soc. Am. 58, 113 (1968).

37. T.C. Hall, Jr., and F.E. Blacet, J. Chem. Phys. 20, 1745 (1952).

38. A.E. Douglas and K.P. Huber, Can. J. Phys. 43, 74 (1965).

39. Alan Harker, Lawrence Berkeley Laboratory Report LBL-1114 (Ph.D. thesis, unpublished).

40. D.G. Fouche, A. Herzenberg, and R.K. Chang, J. Appl. Phys. 43, 3846 (1972).

41. A.E. Douglas, J. Chem. Phys. 45, 1007 (1966).

42. G. Herzberg, Molecular Spectra and Molecular Structure, Vol. III (D. Van Nostrand, Princeton, 1966), p. 602.

43. Ibid., p. 106.

44. E.T. Arakawa and A.H. Nielsen, J. Mol. Spect. 2, 413 (1958).

45. Daivd M. Dennison, Rev. Mod. Phys. 3, 280 (1931).

46. P.B. Sackett and J.T. Yardley, Chem. Phys. Lett. 9, 612 (1971).

47. R. Solarz and D.H. Levy, J. Chem. Phys. 60, 842 (1974).

48. A.W. Tucker, M. Birnbaum, and C.L. Fincher, Appl. Optics 14, 1418 (1975).

49. F.S. Goulding, J.M. Jaklevic, and B.M. Loo, Report UCID-3767, Lawrence Berkeley Laboratory, University of California, Berkeley, CA 94720; Report EPA-650/2-75-048, U.S. Environmental Protection Agency, Washington, DC 20460 (April 1975).

50. F. Tuinstra and J.L. Koenig, J. Chem. Phys. 53, 1126 (1970).

51. S.A. Solin and R.J. Kobliska, in Proceedings of 5th International Conference of Amorphous Liquids and Semiconductors (Taylor and Francis, London, 1974), p. 1251.

52. T. Novakov, S.G. Chang, and A.B. Harker, Science 186, 259 (1974); S.G. Chang and T. Novakov, Atmos. Environment 9, 495 (1975).

PUBLICATIONS

1. P. Robrish, H. Rosen, O. Chamberlain
"Study of the quenching of inelastic light scattering near an isolated resonance in I_2 vapor"
Phys. Letts. 51A, 434 (1975).

2. H. Rosen, P. Robrish, O. Chamberlain
"Feasibility of the remote detection of pollutants using resonance Raman scattering"
"Appl. Optics 14, 2703 (1975).

3. A. Mysyrowicz, A.J. Schmidt, Y.R. Shen, P. Robrish, H. Rosen
"High excitation luminescence of CdS generated by photons with less energy than the bandgap"
Solid State Commun. 17, 523 (1975).

4. P. Robrish, H. Rosen
"Observation of intense and sharp structures in the excitation spectrum of NO_2"
Chem. Phys. Letts. 37, 156 (1976).

5. H. Rosen, P. Robrish, and G. Jan de Vries
"Design of a simple and inexpensive gated integrator"
Rev. Sci. Instrum. 46, 1115 (1975).

6. P. Robrish, H. Rosen
"Study of the spectroscopy of NO_2 by selective excitation with a tunable laser"
Lawrence Berkeley Laboratory Report LBL-3229.

7. Y. Haas, P.L. Houston, J.H. Clark, C.B. Moore, H. Rosen, P. Robrish
"Long-lived $K_a = 0$ $^2B_1$ states of NO_2"
J. Chem. Phys. 63, 4195 (1975).

8. H. Rosen, P. Robrish
"Modulated fluorescence as a possible *in situ* monitor for NO_2"
Lawrence Berkeley Laboratory Report LBL-4470; submitted to Appl. Optics.

9. H. Rosen, T. Novakov
"Application of Raman scattering to the characterization of atmospheric aerosol particles"
Lawrence Berkeley Laboratory Report LBL-5228; submitted to Nature.